Tucholke, B.E., Sibuet, J.-C., Klaus, A., et al., 2004
Proceedings of the Ocean Drilling Program, Initial Reports Volume 210

4. SITE 1277[1]

Shipboard Scientific Party[2]

SITE SUMMARY

Hole 1277A
Latitude: 45°11.8002′N
Longitude: 44°22.5999′E
Time on site: 55.00 (1800 hr, 2 Sep–0100 hr, 5 Sep 2003)
Seafloor (drill pipe measurement from rig floor, mbrf): 4639.4
Distance between rig floor and sea level (m): 11.2
Water depth (drill pipe measurement from sea level, m): 4628.2
Total depth (drill pipe measurement from rig floor, mbrf): 4819.7
Total penetration (m): 180.3
Total length of cored section (m): 76.4
Total core recovered (m): 29.24 (not including 2.29 m from wash Core 210-1277A-1W)
Core recovery (%): 38
Total number of cores: 8
Total number of drilled intervals: 1
Total length of drilled intervals without coring (m): 103.9

With only 3 days of Leg 210 remaining, we moved 40 km southeast of Site 1276 and drilled into the crest of a prominent basement ridge that we call the Mauzy Ridge ("mauzy" is a Newfoundland word for foggy or misty) at Site 1277 (Fig. **F8B,** p. 49, in the "Leg 210 Summary" chapter; Figs. **F20, F21**). The crust here is just on the young side of a magnetic anomaly identified as M1, and it is characterized by a series of high-amplitude, margin-parallel basement ridges (see **Shillington et al.,** this volume). These features suggest that it is oceanic crust formed by early seafloor spreading in the Newfoundland Basin. We drilled Site 1277 to test this inference and to determine the nature of the basement.

Because of the limited time available, we drilled without coring through the thin sediments above the basement ridge. Sediment thick-

[1]Examples of how to reference the whole or part of this volume.
[2]Shipboard Scientific Party addresses.

Ms 210IR-104

ness estimated from multichannel seismic (MCS) stacking velocities prior to drilling suggested a sediment thickness of 132 m, so we planned to drill without coring to 100 meters below seafloor (mbsf). While drilling to this depth we encountered hard layers at 85–89 mbsf and 97.5–100 mbsf, and the recovered "wash core" (210-1277A-1W) contained basaltic and gabbroic debris. Thus, the "basement" surface observed in the seismic reflection record (Figs. F20, F21) may be as shallow as 85 mbsf.

We cored from 103.9 mbsf (wash core) to 180.3 mbsf and recovered a spectacular section of heterogeneous igneous and sedimentary rocks. These rocks include magmatically differentiated gabbros of variable grain size and extent of hydrothermal alteration, together with fine- to coarse-grained sediments that are cemented with calcite spar. Most or all of these rocks reached their present location as mass flows. In addition, the deepest four cores (below ~142.1 mbsf) are dominantly serpentinized peridotite, with minor gabbro and a cataclastic damage zone at the top of this unit. There are also minor intrusive rocks and abundant, mainly calcite, veining similar to Alpine ophicalcites.

The presence of serpentinized peridotite basement indicates that mantle rocks were tectonically exhumed to the seafloor, and they were then covered by thin basalt flows and clastic sediments. These features are characteristic of very slow spreading ocean crust with limited magma supply and extreme tectonic extension. Our results suggest that at least this section of ocean crust in the Newfoundland Basin was formed at a very slow spreading rate.

OPERATIONS

Transit to Site 1277 (Proposed Site NNB-04A)

We began the transit from Site 1276 to Site 1277 at 1530 hr on 2 September. The beginning of the transit was delayed by 45 min because of a problem with the ship's propulsion control system. Once the problem was resolved, the ship was under way at 1615 hr. After a transit of 21 nmi, we arrived at Site 1277 at 1800 hr. The ship was positioned over the site using the Global Positioning System, and the thrusters were lowered by 1815 hr.

Site 1277

Our aim at Site 1277 was to sample 30 m of sediment immediately above basement and then core into basement of a shallowly buried ridge before we had to leave for St. John's. Basement was estimated to be 136 mbsf, so we decided to drill without coring to 100 mbsf and then core until time ran out. Table T1 shows a coring summary for Site 1277.

T1. Coring summary, Site 1277, p. 36.

Hole 1277A

We assembled a rotary core barrel bottom-hole assembly and started lowering it the seafloor at 1830 hr on 2 September. We attached the top drive and deployed a wash core barrel (0230 hr on 3 September) in preparation for drilling. The bit tagged the seafloor at 0300 hr at 4639.4 mbrf. We drilled with the wash core barrel in place from 0 to 103.9 mbsf. Hard intervals were penetrated at 85–89 and 97.5–100 mbsf. The

wash core barrel was retrieved, and it recovered 2.29 m of basement-related rocks, mostly basalts.

Cores 2R to 9R penetrated 103.9–180.3 mbsf and recovered 29.24 m (recovery = 38%). Coring parameters were WOB = 20,000 lb, bit rotation = 70 rpm, torque = 175 A, and circulation = 70 spm at 800 psi. The rate of penetration was 5.5 m/hr. Cores 6R to 8R were taken without plastic core liners to try to minimize core jamming and, hence, low recovery that we were experiencing. The active heave compensator was run while cutting Cores 6R and 8R. We circulated 70 bbl of mud after Core 6R. The final core of Site 1277, Leg 210, and Ocean Drilling Program (ODP) (Core 9R) was recovered on the rig floor at 1200 hr on 4 September. The *last core of ODP* was truly spectacular—a 10.5-m (recovery = 106%) core consisting of green and brown serpentinized peridotite with calcite veins.

We removed the top drive at 1300 hr and began to retrieve the drill string. The seafloor positioning beacon was recovered and back on board at 1500 hr on 4 September. The bit cleared the rig floor at 2345 hr. The drill collars were taken apart, and the ship was secured for transit at 0100 hr on 5 September.

Transit to St. John's, Newfoundland

We began the transit to St. John's at 0100 hr on 5 September. After traveling 374 nmi, the last scientific expedition of the Ocean Drilling Program concluded with the last line ashore at 1500 hr on 6 September 2003.

IGNEOUS AND METAMORPHIC PETROLOGY

Site 1277 is located atop a basement ridge (Mauzy Ridge) beneath a thin cover of sediment. The main objective at this site was to recover basement. For this reason, Hole 1277A was drilled without coring to 103.90 mbsf. It was predicted that the bit would still be ~30 m above the anticipated sediment/basement contact at that depth. While this upper section was drilled, a "wash" core barrel was in place. When retrieved, the core barrel contained 2.29 m of fractured igneous rock and associated volcaniclastic sediments (Core 210-1277A-1W) that were indistinguishable from the rock in the top of Core 2R. Drilling records indicate that hard zones were encountered at 85–89 and 97.5–100 mbsf (see **"Operations,"** p. 2). Thus, the rock recovered in Core 210-1277A-1W most likely came from depths between 85 and 103.90 mbsf. We define the top of Unit 1 to be at the shallower depth of 85 mbsf. Two lithologic units are recognized in Hole 1277A. Because sedimentary units cored at this site are interbedded with, and derived from, rock types characteristic of basement at this site, we discuss all the sedimentary, igneous, and structural features together in this section (see piece logs in **"Site 1277 Visual Core Descriptions"**).

Unit 1 is an igneous–sedimentary succession of alternating basalt flows with hyaloclastites (altered volcanic glass) and laminated sediments within neptunian fissures (~50%); these rocks compose ~50% of the unit. In addition, coarse matrix-supported breccias (20% of unit) contain a wide variety of clasts of gabbro and serpentinite, and variably deformed and differentiated gabbros (20%) appear to represent large clasts or fragments in matrix-supported breccias. There are also minor sandstones, locally ferruginous (<10%).

Unit 2 contrasts with Unit 1 in that it consists almost entirely of variably deformed serpentinized peridotite (~95%) cut by magmatic and calcite veins. The lack of sediments and lavas, as well as the occurrence of a steeply inclined and locally intense high-temperature foliation within the serpentinized peridotite (Fig. F1), suggest that this unit represents true basement (i.e., massive mantle and crustal rocks that are in situ).

The serpentinized peridotite drilled at Site 1277 is interpreted to be basement that represents tectonically exhumed mantle. This interpretation is compatible with the observation that the serpentinite in Unit 2 shows pervasive brittle deformation and hydrothermal alteration that decreases downhole. The downhole decrease in alteration may explain increasing core recovery with depth, from <9.28% at the top of the serpentinite (Core 210-1277A-6R) to 105.73% at the bottom of the hole (Core 9R, the last core of ODP). After exhumation, the serpentinites were buried by lavas and basement-derived sediments of Unit 1. Postcruise studies may help to confirm our inference that tectonic exhumation of Unit 2 was coincident with sedimentation and volcanism in Unit 1 and also to clarify how the clastic sediments were preserved on what is now a basement high.

Unit 1

Interval: 210-1277A-1W, 0 cm, through Section 5R-3
Curated depth: 0–142.10 mbsf (length recovered = 12.93 m; average recovery = 33.94%, excluding Core 210-1277A-1W)
Interpreted depth: 85–142.10 mbsf
Lithology: basalt flows associated with hyaloclastite and clastic sediments in neptunian fissures, gabbro and serpentinized peridotite (mostly as clasts in a sedimentary matrix), and fine- to coarse-grained clastic sediments

Figure F2A summarizes the main lithologies of Unit 1. Details are given in the visual core descriptions for this site (see "Site 1277 Visual Core Descriptions"). Low recovery in Unit 1 (~35%, excluding Core 210-1277A-1W) means that the lithologic record is very fragmented and incomplete, so it may be biased toward certain rock types. Examples of typical occurrences of each rock type are described and briefly interpreted below.

Basalt Flows with Associated Hyaloclastites and Sediments in Neptunian Fissures

There are three intervals of basalt flows (intervals 210-1277A-1W-1, 61 cm, through 1W-2, 75 cm; 2R-2, 68 cm, through 3R-4, 60 cm; and 5R-1, 3–135 cm) interbedded with clastic sediments (Figs. F2, F3, F4). Together, the flows form ~50% of Unit 1. The thickest example in Cores 210-1277A-2R and 3R includes one discrete flow at the base and several overlying, possibly composite flows. The lowest flow overlies sediments with a contact that was recovered intact; it has a chilled top and shows a gradual downhole increase in crystal size within the flow, from aphanitic to fine grained. The top of the flow is marked by ~1 cm of vesicular basalt grading into green, crustose, laminar hyaloclastite up to 1 cm thick. Some fragments of hyaloclastite are spalled off into an overlying thin interflow unit of clastic sediment that is several centimeters thick.

F1. Serpentinized peridotite with high-temperature foliation, p. 14.

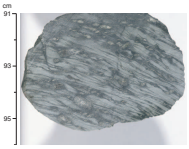

F2. Lithologies and structural features, p. 15.

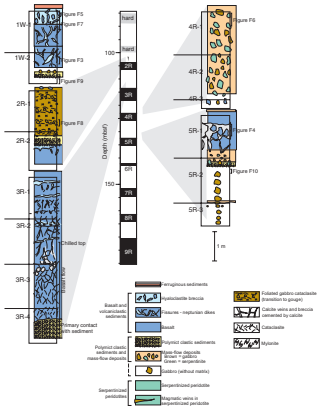

F3. Fissures filled with hyaloclastite and calcite spar, p. 17.

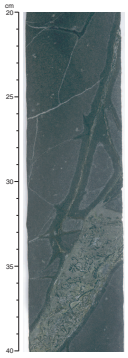

F4. Brecciated basalt with calcite cement, p. 18.

Most of the flows observed in the three intervals are cut by irregular fractures or fissures as wide as 1 cm that are filled with calcite-spar cement. Some incompletely filled fractures are lined with dogtooth calcite spar (Fig. F4). Larger fissures (up to 4 cm) are also present and are filled with sediment composed of poorly sorted silt- to granule-size clastic sediments derived from the basalts (Fig. F3). In several fissures, internal sediment has planar lamination and there are also occasional elliptical to elongate fragments of concentrically laminated hyaloclastite. In one interval, the basalt clasts and matrix are stained a reddish color, especially at the margins of the clasts, which resulted from alteration at or near the seafloor.

Chilled margins at the tops of all flows and gradual downhole increases in crystal size in the flows indicate that the basalts are relatively intact and are not large fragments within a sedimentary breccia. Hyaloclastites between the flows probably originated from the chilled tops of the flows. Hyaloclastite and basaltic sand filtered down into cracks in the flows; these sediment-filled fissures are interpreted as neptunian dikes. They are filled with carbonate, reddish iron oxide, and sediments, and they have a jigsawlike appearance. There are two generations of clastic-sediment fill. The first is soft, brown, unstructured, fine-grained ferruginous or ferromanganese-rich sediment (Fig. F5). The second generation, which cuts the first generation, is pale gray, altered silt- and granule-size clastic sediment that shows a vague subhorizontal lamination defined by coarser sand grains.

F5. Uppermost lithologies in Hole 1277A, p. 19.

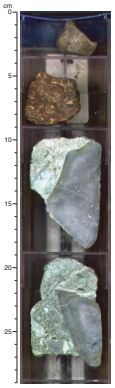

Gabbro and Serpentinized Peridotite (Mostly Clasts in Sedimentary Matrix)

There are several intervals of disorganized breccia that contain subangular to subrounded clasts of gabbro and serpentinized peridotite (e.g., Sections 210-1277A-4R-1 through 4R-2 and 5R-1, 125 cm, through 5R-2, 29 cm) (Fig. F6). The breccias form ~20% of the recovery in Unit 1, and the clasts constitute ~30% of the breccia. The serpentinized peridotite clasts preserve a great variety of structures (Fig. F6), ranging from high-temperature peridotite mylonite (e.g., intervals 210-1277A-4R-1, 8–25 cm) to undeformed massive serpentinite.

A few gabbro clasts preserve a mylonitic structure, although most gabbro preserves primary magmatic textures. Most of the gabbro is magmatically differentiated and contains plagioclase, pyroxene, brown amphibole, and illmenite; no olivine was observed. Secondary mineral phases include chlorite, tremolite, and calcite. Most gabbro clasts are less altered than equivalent small intrusive gabbro veins in the underlying serpentinized peridotite of Unit 2.

The breccia matrix (~70% of the rock) is composed of finer-grained subangular to subrounded clasts of serpentinite and gabbro that form a reddish brown silty sandstone (Fig. F6). This is cemented by calcite spar, which may be a later hydrothermal precipitate. The breccias are unsorted, and there is a wide range of clast sizes. Like the lava flows, the breccias are cut by calcite veins, some as wide as 2 cm. Many larger clasts have rims of calcite spar up to several millimeters thick. The breccias are matrix supported and have a polymict, disorganized fabric; these features suggest emplacement by mass-flow processes.

There are two intervals of gabbroic rocks that are not associated with a sedimentary matrix; these are interpreted as large clasts or fragments within mass-flow deposits. The upper of the two intervals (Sections 210-1277A-2R-1, 13 cm, through 2R-2, 40 cm) is >177 cm thick and is

F6. Serpentinite and gabbro mass-flow deposits, p. 20.

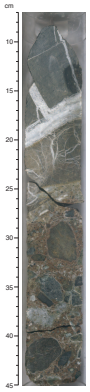

composed of strongly altered and cataclastically deformed gabbro (Fig. F7). The overall gabbroic texture is well preserved, but locally it is disrupted and shows plagioclase and pyroxene porphyroclasts within a foliated chlorite-rich matrix. Individual porphyroclasts are as large as several centimeters, are angular to well rounded, and have altered margins. A weak foliation is defined by a preferred orientation of the fabric within the chloritic matrix and by a crude alignment of mainly the smaller (<2 cm) elongate porphyroclasts.

The lower interval (Sections 210-1277A-5R-2, 68 cm, through 6R-1, 52 cm) is a foliated gabbro cataclasite. It is considered to have a tectonic rather than sedimentary origin, and it is described as part of Unit 2 (Fig. F2B) (see "Foliated Cataclasites and Gouges," p. 7, in "Unit 2").

F7. Strongly altered gabbro, p. 21.

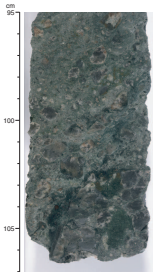

Fine- to Coarse-Grained Clastic Sediments

Several intervals of locally ferruginous clastic sediment appear in Unit 1, forming less than ~10% of the overall recovery. These beds are all less than ~50 cm thick and have variable sedimentary textures and structures. Several examples are described below.

In intervals 210-1277A-1W-2, 90–104 cm (Fig. F8), 2R-2, 41–68 cm, and 3R-4, 61–108 cm, there is calcite-cemented, polymict breccia conglomerate with angular to rounded clasts as large as 2 cm. The highest of these intervals is normally graded, ranging from pebbles to coarse sand, with a few scattered larger clasts toward the top. The clasts are dominantly mafic (~60%) and ultramafic (~40%). The lower two intervals consist of granule- to pebble-size grains of gabbro and serpentinite set in a poorly sorted matrix of siltstone to sandstone consisting of the same lithologies. The clasts are subangular to subrounded. There is postdepositional calcite replacement of the matrix in these breccias.

A 40-cm-thick sedimentary breccia in interval 210-1277A-1W-1, 10–61 cm (Figs. F5, F9), is composed of basalt fragments randomly distributed in a matrix of greenish, unsorted, clastic sediment cemented by calcite spar. The angular clasts are mainly unaltered aphyric basalt (up to ≥10 cm in size) together with elongate hyaloclastite fragments.

In interval 210-1277A-5R-2, 33–42 cm (Fig. F10), there is a single piece of finely laminated, reddish to purple and gray, fine- to medium-grained, graded sandstone that may be either a sedimentary bed or the sedimentary fill of a large neptunian dike.

Interval 210-1277A-1W-1 (Piece 2A, 5–9 cm) contains a single piece of well-indurated, brown, clastic sediment impregnated with ferromanganese oxide (Fig. F5). Coarse sand grains in this piece consist of variably altered basalt, feldspar, and bioclasts that include strongly altered, agglutinated benthic foraminifers. These grains are enveloped by a microlaminated ferromanganese crust showing centimeter-scale, laterally linked, irregular, and wrinkled domes. We interpret this distinctive ferruginous sediment to be part of a thin authigenic cap on the basement high.

F8. Polymict clastic sediment, p. 22

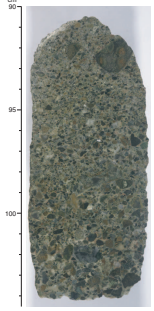

F9. Hyaloclastite cut by a neptunian fissure, p. 23.

F10. Well-laminated and graded sandstone cut by calcite-filled fractures, p. 24.

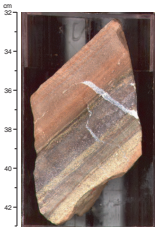

Unit 2

Interval: 210-1277A-6R-1, 0 cm, through Section 210-1277A-9R-8
Depth: 142.10–180.30 mbsf
Lithology: tectonized gabbro at the top, tectonized serpentinized peridotites, and both magmatic and hydrothermal veins

The top of Unit 2 is defined by the downward disappearance of sedimentary rocks and basalt flows. It consists of a thin 50-cm-thick interval of strongly altered and tectonized gabbro that overlies serpentinized peridotite. The degree of serpentinization is >95% throughout Unit 2. Downhole, the intensity of brittle deformation decreases and a transition to serpentinized peridotite mylonite is observed. The peridotite shows a complex history of hydrothermal alteration and polyphase veining. This includes intrusion of highly differentiated plutonic rocks. At the time of the intrusions, the peridotite was already serpentinized, as indicated by complex reaction rims of talc, amphibole, and calcite at the interface between the magmatic veins and the altered ultrabasic rock. Extensive calcite veining is also observed throughout the succession.

Figure F2B summarizes Unit 2. Details are given in the core descriptions for this site (see "Site 1277 Visual Core Descriptions"). Examples of typical occurrences of each rock type are described below.

Foliated Cataclasites and Gouges

The top of Unit 2 (interval 210-1277A-6R-1, 0–52 cm) (Fig. F2B) consists of greenish gray heterogeneous foliated cataclasites that comprise ~5% of Unit 2. The rocks contain angular to subrounded gabbro clasts in a fine groundmass formed from abraded minerals (formerly plagioclase and pyroxene) altered to albite, chlorite, and calcite. Fragmented spinel grains derived from mantle peridotite were also observed. Elongated clasts and minerals within these rocks define a vague foliation, and the rocks are interpreted to be tectonic rather than sedimentary. The occurrence of foliation and the absence of carbonate cement, such as that found in Unit 1 sediments, support this observation. The presence of spinel within the gabbroic rocks suggests that ultramafic rocks were involved in the formation of the foliated cataclasites. We tentatively suggest that both mafic and ultramafic rocks were deformed in a shear zone as they were exhumed.

Serpentinized Peridotite

Serpentinized peridotites were recovered from Section 210-1277A-6R-1, 52 cm, to the bottom of the hole. They comprise ~95% of Unit 2. The uppermost interval in Cores 210-1277A-6R to 8R is composed of serpentinized peridotite that generally is strongly brecciated and calcite veined, although the rocks commonly preserve a high-temperature foliation (Figs. F1, F11). Below this, primary mantle fabrics are better preserved in Core 210-1277A-9R, which contains a spectacular intact section of serpentinized peridotite mylonite (105.73% recovery) (Figs. F12, F13, F14). The original mineralogical composition of this peridotite is masked by serpentinization (locally up to 100%), and crystal size has been strongly reduced by dynamic recrystallization. Visual inspection of the core reveals 5%–10% orthopyroxene porphyroclasts with minor spinel, but this may be an underestimate of the total amount of pyroxene. Most of the spinel crystals range from needle shaped to vermicular to small aggregates intergrown with orthopyroxene (<1 mm). Postcruise investigation will be needed to define the composition and nature of these rocks more precisely.

Well-developed mylonitic foliation in Core 210-1277A-9R is defined by preferred elongation of orthopyroxene porphyroclasts (<1 cm in size) with aspect ratios of 4:1 and higher. Unfortunately, the matrix is completely serpentinized and no primary microstructures are observed.

F11. Foliated serpentinized peridotite with anastomosing veins, p. 25.

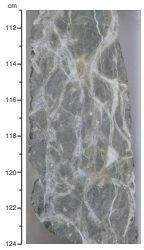

F12. Foliated serpentinized peridotite, p. 26.

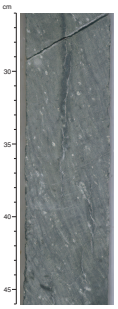

F13. Serpentinized peridotite cut by calcite veins, p. 27.

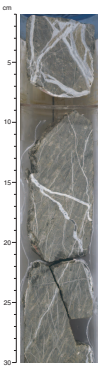

F14. Serpentinized peridotite cut by plagioclase-bearing magmatic veins, p. 28.

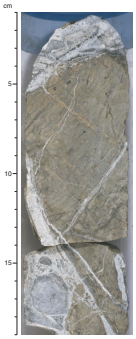

Thin section observations show that the mylonitic foliation is overgrown statically by serpentine, indicating that the deformation predates the serpentinization and is probably unrelated to final exhumation of these rocks to the seafloor. The mylonitic foliation dips at angles as much as 80° and is cut by later subhorizontal brittle shear zones, which also suggests that the foliation is an early fabric.

Colors ranging from orange green to greenish gray are observed in Core 210-1277A-9R. They are unrelated to the underlying structures or primary mineralogical composition. Thin section observations indicate that they are controlled by variable intensity of alteration.

The serpentinized peridotite in Unit 2 is intruded by magmatic veins that show complex reactions with the ultramafic host rock (e.g., Sections 210-1277A-9R-1 and 9R-2) (Fig. F14). Within these reaction rims, the growth of talc and amphibole over previously serpentinized peridotite indicates that the veins postdate serpentinization. The veins show a polyphase alteration history, ending with fracturing and precipitation of calcite that filled the veins or was deposited at their edges. In some places, calcite was precipitated as veins and as calcite cement in yellowish brown serpentinite breccia (e.g., intervals 210-1277A-6R-1, 52–68 cm, and 7R-1, 0–20 cm). These breccias have a jigsawlike fabric but no sedimentary structure, showing that they are tectonic rather than sedimentary in origin.

Although pervasive veining in Unit 2 records several stages of fracturing and mineral precipitation, there is no clearly defined succession in terms of vein structure, size, or composition. Many of the smaller veins that cut the serpentinized peridotite are composed of calcite with subordinate talc and magnetite. The earlier veins tend to be relatively gently dipping (e.g., in interval 210-1277A-8R-2, 0–100 cm). In contrast, the larger veins (reaching 1.5 cm wide) are mainly subvertical and infilled with calcite spar (e.g., intervals 210-1277A-8R-1, 1–27 cm, and 108–119 cm).

Calcite veins in both the basalt flows of Unit 1 and the underlying serpentinized peridotites of Unit 2 suggest that fracturing and precipitation of calcite occurred after both units were in place. Therefore, calcite veins are considered to be the youngest structures observed in the basement rocks at Site 1277. The calcite-veined serpentinites are comparable to certain ophicalcites known from ultramafic sections of the western Tethyan region (e.g., Alps and Liguria) (Bernoulli and Weissert, 1985).

BIOSTRATIGRAPHY

No shipboard biostratigraphic analysis was conducted on the few sedimentary rocks recovered at Site 1277 because no suitable materials were recovered.

Agglutinated benthic foraminifers occur in a single piece of indurated ferruginous sediment (Sample 210-1277A-1W-1, 5–9 cm) overlying igneous rocks at Site 1277 (Fig. F5). The few poorly preserved specimens include planispirally coiled forms with numerous chambers and alveolar internal walls similar to those in the family Cyclamminidae. There are also encrusting(?) tubelike forms possibly belonging to the family Ammodiscidae. In addition, several tiny planktonic foraminifers were observed in a dark-colored sedimentary clast. No age-diagnostic taxa were observed.

PALEOMAGNETISM

We made pass-through magnetometer measurements and magnetic susceptibility measurements on all split-core archive sections at 2-cm intervals. In order to isolate the characteristic remanent magnetization (ChRM), we subjected the cores to alternating-field (AF) demagnetization. The half cores were demagnetized up to 60 mT. We analyzed the results in Zijderveld diagrams (Zijderveld, 1967) and calculated the ChRM directions using principal component analysis (Kirschvink, 1980). In addition, we determined magnetic susceptibility on all whole cores from Site 1277 at 2.5-cm intervals as part of the multisensor track (MST) analysis and measured split-core sections at 2-cm intervals with the point-susceptibility meter (archive multisensor track). No discrete shipboard paleomagnetic samples were taken because of time limitations at the end of the leg.

Paleomagnetic data obtained at Site 1277 exhibit significant variations in demagnetization behavior among various recovered lithologies (Fig. **F15;** Tables **T2, T3, T4**). Variations in magnetic susceptibility generally parallel the variations in natural remanent magnetization (NRM) intensity (Fig. **F15**). Drilling-induced remagnetization is observed, but it has much less effect than it did for sediments in Hole 1276A. In most instances, we were able to remove this remagnetization with 10- to 20-mT AF demagnetization and to isolate the ChRM direction using higher field intensities (Fig. **F16**). Paleomagnetic measurements indicate that the greenish gabbro cataclasite in Core 210-1277A-2R has the lowest NRM intensity (~0.02–0.3 A/m) in contrast with the relatively fresh aphyric basalt in Cores 1W, 3R, and 5R (~1–4 A/m), gabbro at the base of Core 4R and in the lower part of Core 5R (0.2–0.5 A/m), and serpentinized peridotite in Core 9R (1–9 A/m).

The basalts appear to record a stable component of magnetization with normal inclinations (~45°). On the other hand, the cataclasite in Core 210-1277A-2R displays variable inclinations (from positive shallow to even negative shallow), consistent with the fact that it is tectonized (see **"Igneous and Metamorphic Petrology,"** p. 3). The gabbros and adjacent sediments in Cores 210-1277A-4R and 5R have the same stable inclination values of ~40°, which agree with the inclination values observed from the basalt. This is consistent with expected Cretaceous inclinations for this region.

The serpentine peridotites in Core 210-1277A-9R show a variable degree of overprinting, but AF demagnetization easily removed the overprint and allowed isolation of the ChRM direction (Fig. **F16**). ChRM inclinations obtained from different parts of long coherent core pieces generally agree within a few degrees and cluster around a mean of 40°, similar to inclination values in the basalt and gabbro. The fact that the NRM intensities of the serpentinized peridotite are typically 1–9 A/m suggests that they could significantly contribute to the regional magnetic anomaly. We also observe a distinct difference between the gabbro, which has relatively low magnetic susceptibilities and high median destructive fields (MDFs), and the serpentinized peridotite, which has high susceptibilities and low MDFs (see Table **T4**). This difference can be explained by either the finer magnetic grain size of the gabbro, its higher degree of low-temperature alteration, or a combination of these factors. Shore-based rock magnetic studies on discrete samples will investigate the cause of the downhole variation in rock-magnetic properties.

F15. Magnetic susceptibility, intensity, and inclination, p. 29.

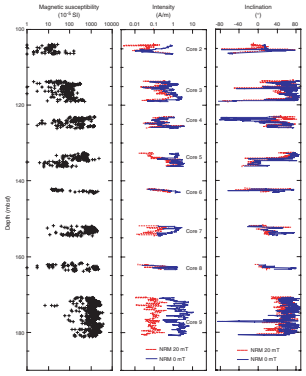

T2. Remanent magnetization intensity and inclination, p. 37.

T3. Magnetic susceptibility, p. 38.

T4. Paleomagnetic characteristics, p. 39.

F16. Zijderveld diagrams, p. 30.

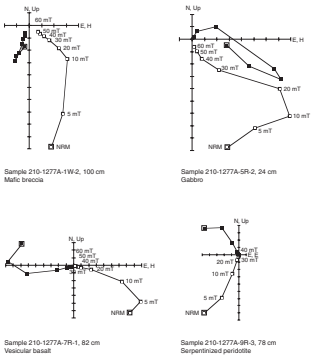

PHYSICAL PROPERTIES

Evaluation of physical properties at Site 1277 included nondestructive measurements of density, porosity, velocity, and thermal conductivity. Horizontal (x- and y-directions) and vertical compressional wave (*P*-wave) velocity (z-direction) were measured on cubes cut from half-core samples. Porosity and density were determined from cylinders shaped from the velocity-determination cubes. Thermal conductivity was measured on lithified half-core samples. Apart from an initial wash core (Core 210-1277A-1W), core recovery commenced at 103.90 mbsf and continued to 180.30 mbsf (Cores 2R through 9R). Because of the urgency to have cores split and made available to the structural and igneous petrology groups, the cores were not measured using the MST.

Density and Porosity

Bulk density, grain density, and porosity at Site 1277 were calculated from the wet mass, dry mass, and dry volume of discrete samples using the moisture and density (MAD) method C (Blum, 1997). These measurements were made on lithified sedimentary and igneous rocks in Cores 210-1277A-2R through 9R (103.90–180.3 mbsf). The majority of samples from Site 1277 are igneous and metamorphic rocks. MAD bulk density and grain density vary by 0.3–0.5 g/cm³ downhole (mean = 2.47 g/cm³ and 2.75 g/cm³, respectively) (Fig. **F17**). Relatively low bulk densities are associated with Cores 210-1277-4R, part of a mass-flow unit, and 9R, which consists of serpentinized peridotite mylonites and cataclasites. Although the majority of porosities are 10%–20%, values range from 2% to 25% (average = 15.9%), reflecting the variably fractured and brecciated nature of most of the recovered section (Fig. **F17**). There is no obvious downhole trend in porosity, and the maximum porosities are associated with the sediments and mass flows of Sections 210-1277A-4R-1 and 4R-2. The lowest porosities are associated with basalts and gabbros of Cores 210-1277A-3R and 5R and with the serpentinized peridotites in Core 7R. Porosities in the serpentinized peridotites range from 9% to 21%. The serpentinized peridotites show remarkably uniform bulk densities (~2.4 g/cm³) and grain densities (~2.66 g/cm³). Grain densities for the basalts and mass flows range between 2.76 and 3.00 g/cm³, and bulk densities range from 2.3 to 2.8 g/cm³.

F17. MAD bulk density, grain density, and porosity measurements, p. 31.

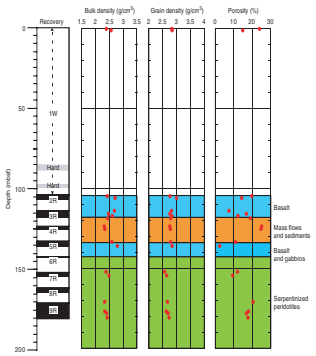

Compressional Wave Velocity

Compressional wave velocities were measured with the *P*-wave sensor 3 (PWS3) contact probe system on ~8-cm³ cube samples of lithified sediments and igneous rocks. The cubes were used to measure velocities in the horizontal (x and y) and vertical (z) directions.

Measured velocities range from 3300 to 6300 m/s (Fig. **F18**). Velocity is lowest (~3270 m/s) in highly altered and veined breccia (Section 210-1277A-4R-2), and it is highest (6325 m/s) in a coarse-grained gabbro (Section 5R-3). Serpentinized peridotites show a range of velocity between ~3300 and 4700 m/s. There is no obvious downhole trend in velocity.

Velocity data in the x-, y-, and z-directions were used to define velocity anisotropy. Velocity anisotropy was calculated as follows:

$$\text{Anisotropy (\%)} = (V_h - V_v)/[(V_h + V_v)/2] \times 100,$$

F18. PWS3 *P*-wave velocity, p. 32.

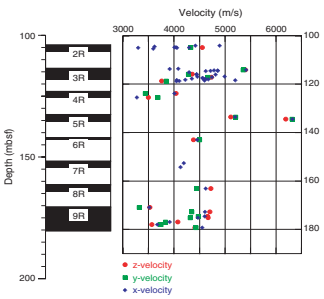

where V_h is the mean horizontal (x and y) *P*-wave velocity and V_v is the vertical (z) velocity. The calculated anisotropy ranges from –9% (altered gabbros) to 6% (sediments) (average = –1.5%).

Thermal Conductivity

Thermal conductivity measurements were made on intact pieces of half-round core of at least 10 cm in length. Thermal conductivity in Hole 1277A ranges from 1.6 to 2.25 W/(m·K) (Fig. F19) with the majority of values ranging from 1.6 to 2.0 W/(m·K) (average = 1.86 W/[m·K]). There is a general increase in thermal conductivity between Core 210-1277A-2R (gabbro cataclasite and basalt) and Core 4R (sediments and mass flows). In contrast, the serpentinized peridotites show a relatively consistent thermal conductivity value of 1.75–2.0 W/(m·K) with depth.

SEISMIC-BOREHOLE CORRELATION

Site 1277 is located on the top of a basement high (Mauzy Ridge) close to interpreted magnetic Anomaly M1. The basement high is part of a margin-parallel ridge, which is apparent from the observed structure in two seismic reflection profiles that cross Site 1277, SCREECH line 2MCS and SCREECH line 206 (Fig. F20). There are no logging data or other concrete tie points between the core and seismic data, and linking seismic data to core data at Site 1277 is difficult. Coring began below an unexpectedly shallow basement surface, so a definitive sediment/basement contact cannot be used as a reference. Even if this boundary had been cored, correlating it to the reflection record would be complicated; the uppermost crust in the seismic section has a "layered" appearance (Fig. F21), which makes identifying the top of basement difficult.

Prior to drilling, basement depth was estimated to be 136 mbsf, based on MCS stacking velocities obtained from the SCREECH survey. During drilling with a wash core to 103.9 mbsf, hard layers were encountered at 85–89 and 97.5–100 mbsf and 2.29 m of basalt, gabbro, and volcaniclastic breccia were recovered in the core. Similar rocks were recovered beginning at 103.9 mbsf in the first rotary core (Core 210-1277A-2R), and serpentinized peridotite was recovered in deeper cores. The shallowest "basement" reflection in the MCS record could be generated by either the layer at 85 mbsf or the layer at 97.5 mbsf. The shallowest irregular "basement-type" reflection beneath onlapping sediments is ~110 ms below the seafloor (Fig. F21). If this correlates to the 85-mbsf hard layer, the seafloor-to-basement interval velocity would be 1545 m/s; if it correlates to the 97.5-mbsf hard layer, the interval velocity would be 1772 m/s.

Below 103.9 mbsf, coring continued for another 76.4 m. To estimate the depth of basement penetration on the seismic record, we used velocities based on laboratory measurements of the cored rocks. The average vertical z-velocity for Site 1277 samples is ~4480 m/s (see "Physical Properties," p. 10). It is likely that this average is a high-end estimate because velocities were not measured on sections of core that were more delicate, including breccias and shear zones, that most likely would have slower velocities. Assuming an average basement velocity of 4000 m/s, our total basement penetration would be a two-way traveltime of 41–48 ms, depending on whether basement is picked at 97.5 or 85 mbsf, respectively. At an average basement velocity of 4450 m/s, to-

F19. Thermal conductivity, p. 33.

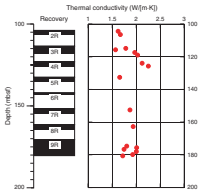

F20. Time-migrated seismic reflection sections, p. 34.

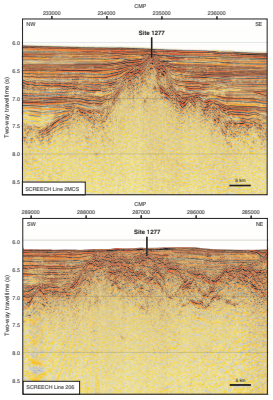

F21. Close-up of seismic reflection section, p. 35.

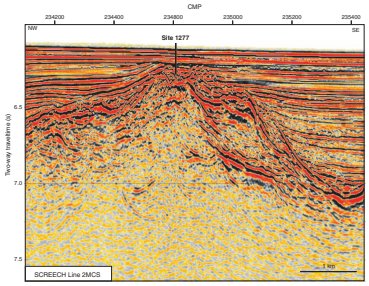

tal basement penetration would be 37–43 ms. All of these estimates place the bottom of the hole within the zone of irregularly layered reflections observed at the top of basement (Figs. F20, F21).

REFERENCES

Bernoulli, D., and Weissert, H., 1985. Sedimentary fabrics in Alpine ophicalcites, South Pennine Arosa Zone, Switzerland. *Geology,* 13:755–758.

Blum, P., 1997. Physical properties handbook: a guide to the shipboard measurement of physical properties of deep-sea cores. *ODP Tech. Note,* 26 [Online]. Available from World Wide Web: <http://www-odp.tamu.edu/publications/tnotes/tn26/INDEX.HTM>. [Cited 2003-09-05]

Kirschvink, J.L., 1980. The least-squares line and plane and the analysis of palaeomagnetic data. *Geophys. J. R. Astron. Soc.,* 62:699–718.

Zijderveld, J.D.A., 1967. AC demagnetization of rocks: analysis of results. *In* Collinson, D.W., Creer, K.M., and Runcorn, S.K. (Eds.), *Methods in Palaeomagnetism:* New York (Elsevier), 254–286.

Figure F1. Serpentinized peridotite preserving a strong high-temperature foliation (interval 210-1277A-8R-1, 91–95.5 cm). Note the asymmetric porphyroblasts composed of altered orthopyroxene (i.e., bastite).

Figure F2. Composite log showing major lithologies and sedimentary and structural features for Hole 1277A. **A.** Unit 1. (Continued on next page.)

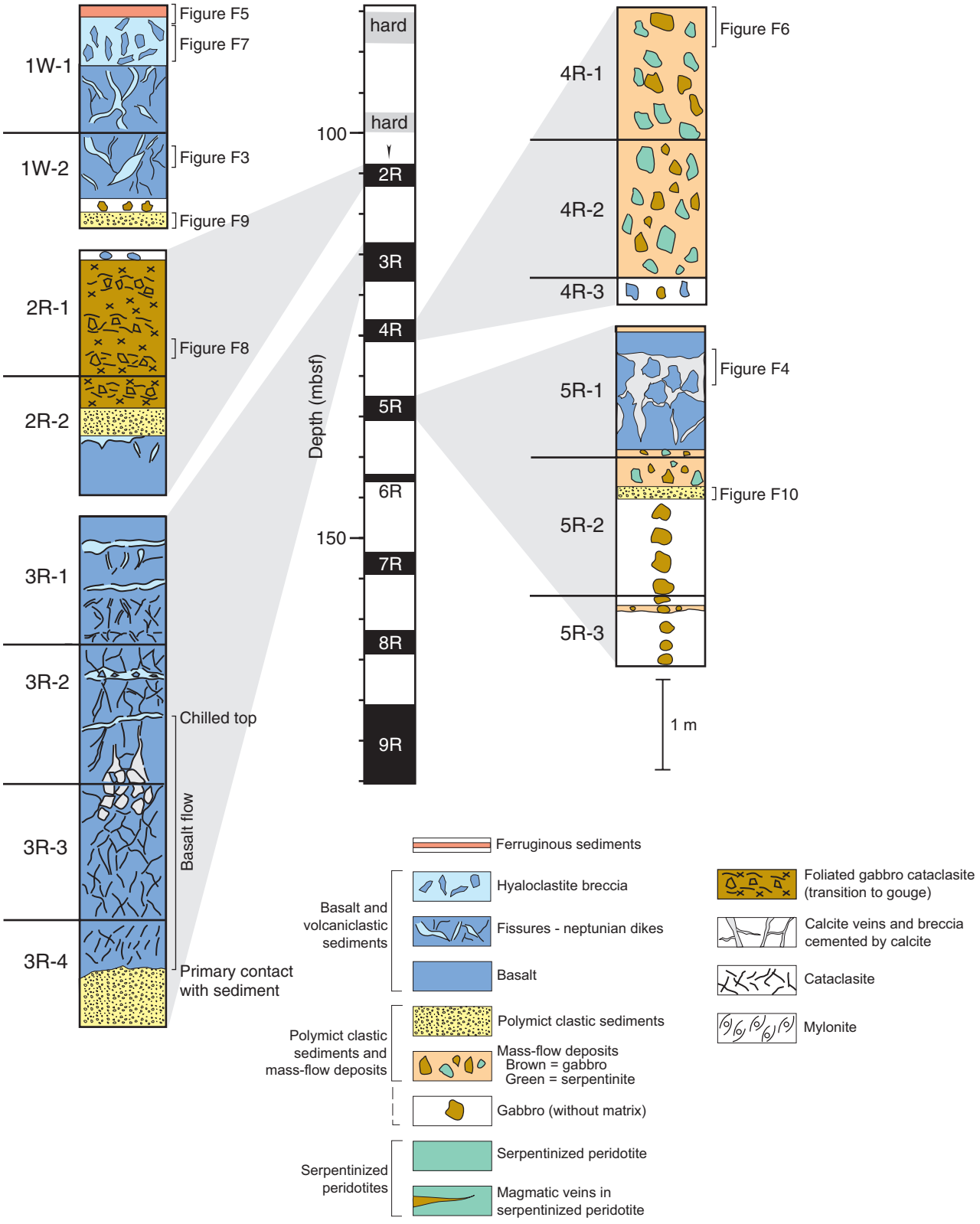

Figure F2 (continued). B. Unit 2.

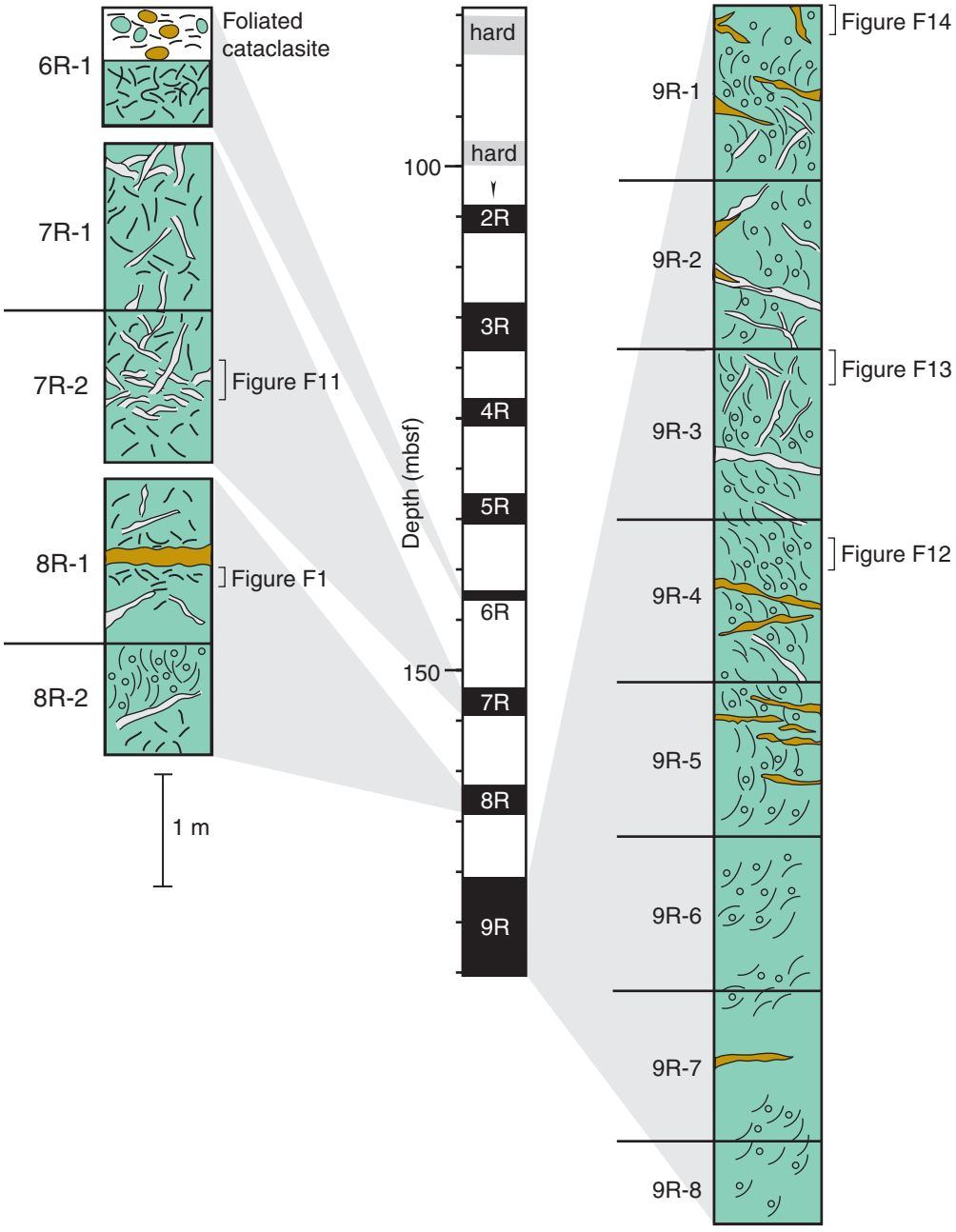

Figure F3. Aphyric basalt containing fissures filled with fragments of hyaloclastite and calcite spar (32–40 cm). Smaller cracks in the upper part of the image (20–29 cm) are filled mainly with calcite spar (interval 210-1277A-1W-2, 20–40 cm).

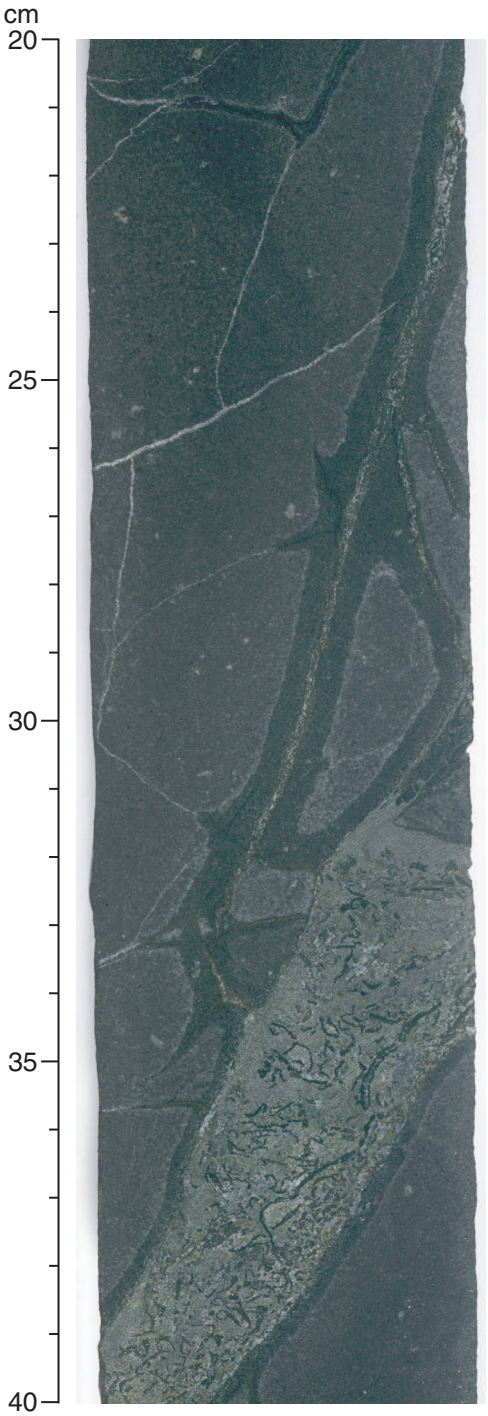

Figure F4. Medium-grained brecciated basalt (interval 210-1277A-5R-1, 24–57 cm). Fractures are filled with basalt clasts, some of which show jigsaw-type textures, within a calcite-spar matrix (pale granular material, 25–38 cm). Note the dogtooth spar in the open fracture at the bottom.

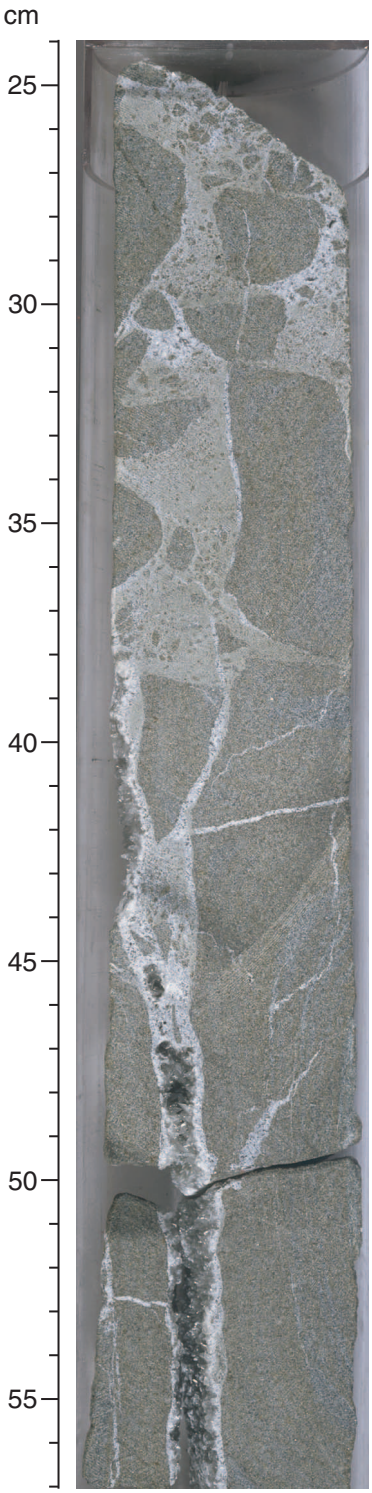

Figure F5. The stratigraphically highest lithologies recovered in Hole 1277A (interval 210-1277A-1W-1, 0–29 cm). The uppermost piece (1–3 cm) is micaceous sandstone that could be derived from overlying sedimentary rocks but might be a glacial dropstone. The rock at 5–9 cm is ferruginous-oxide sediment that has a laminated, stromatolitic, or microbial texture and contains agglutinated benthic foraminifers. The interval from 10 to 28 cm includes two large clasts of aphyric basalt set in hyaloclastite matrix.

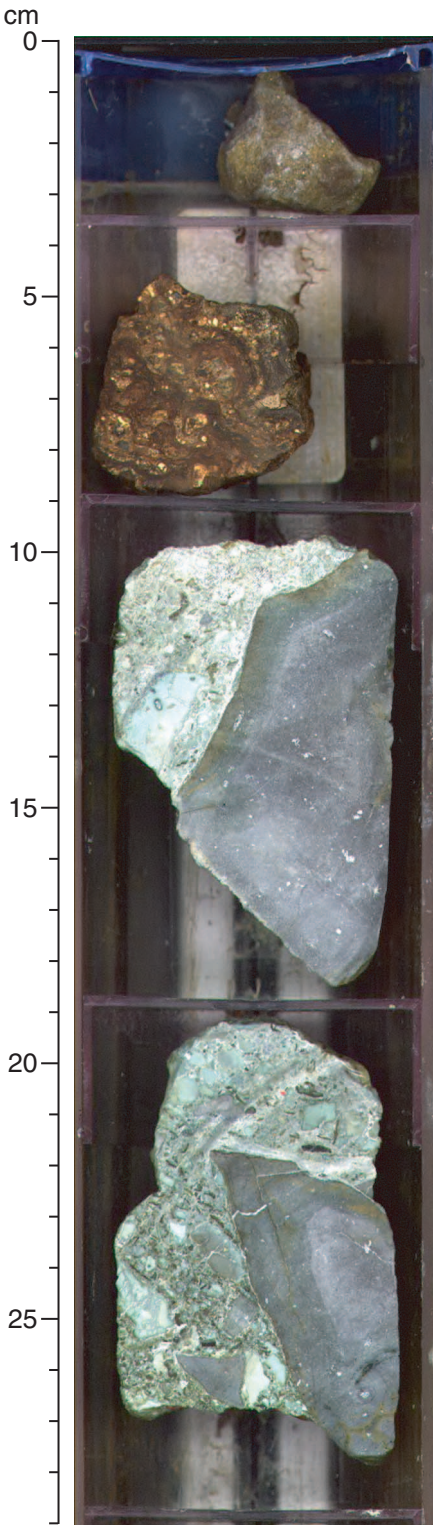

Figure F6. Matrix-supported mass-flow deposits composed of subrounded clasts of serpentinite and gabbro (interval 210-1277A-4R-1, 7–45 cm). Some of the serpentinite clasts (e.g., the large, fractured clast at 8–25 cm and the rounded clast at 40–43 cm) exhibit foliation that is cut by calcite veins, similar to the structure observed in the serpentinites of Unit 2.

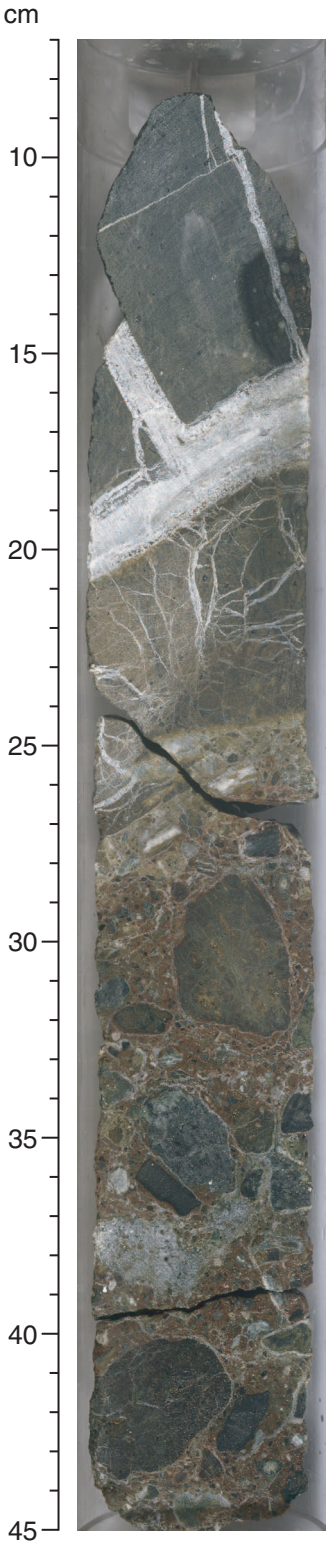

Figure F7. Strongly altered gabbro (interval 210-1277A-2R-1, 95–107 cm) including a transition to disaggregated, vaguely foliated gabbro (upper part). The vague foliation is defined by preferential alignment of altered and elongated plagioclase aggregates lying within a greenish, chloritic matrix. This type of deformation is not observed in the polymict clastic sediments that are present elsewhere in Unit 1, but it is very similar to that observed at the top of Unit 2. This deformed and strongly altered gabbro most likely is a fragment of the underlying basement that has been reworked and emplaced within a sedimentary matrix.

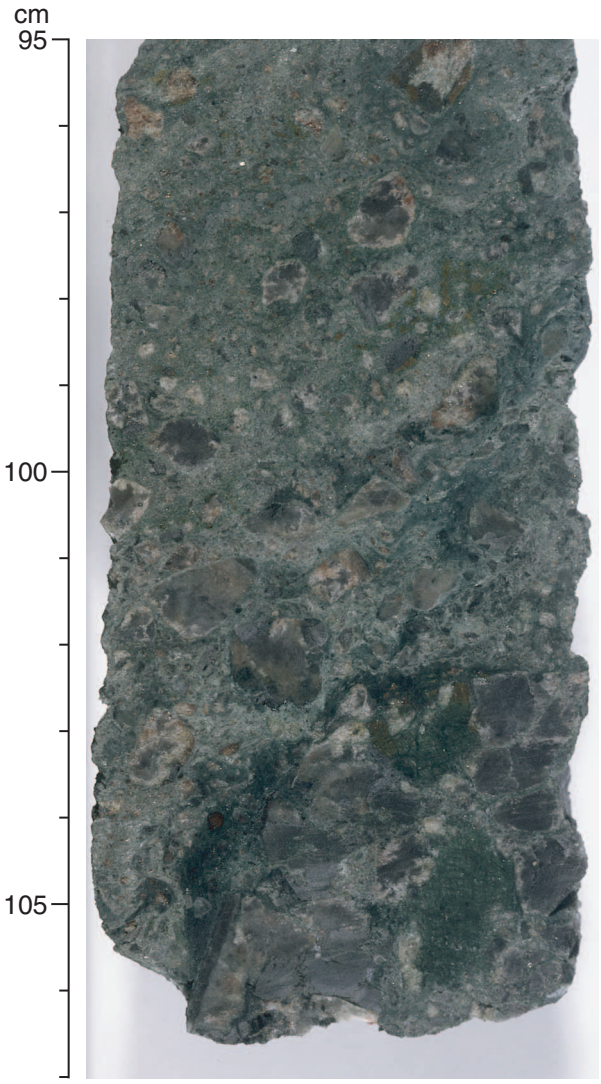

Figure F8. Polymict clastic sediment composed of angular to subrounded clasts of serpentinite and gabbro set in a sparry calcite matrix (interval 210-1277A-1W-2, 90–104 cm). Note the mixture of relatively well rounded and subangular clasts and the unusually large pebble near the top (92–93 cm).

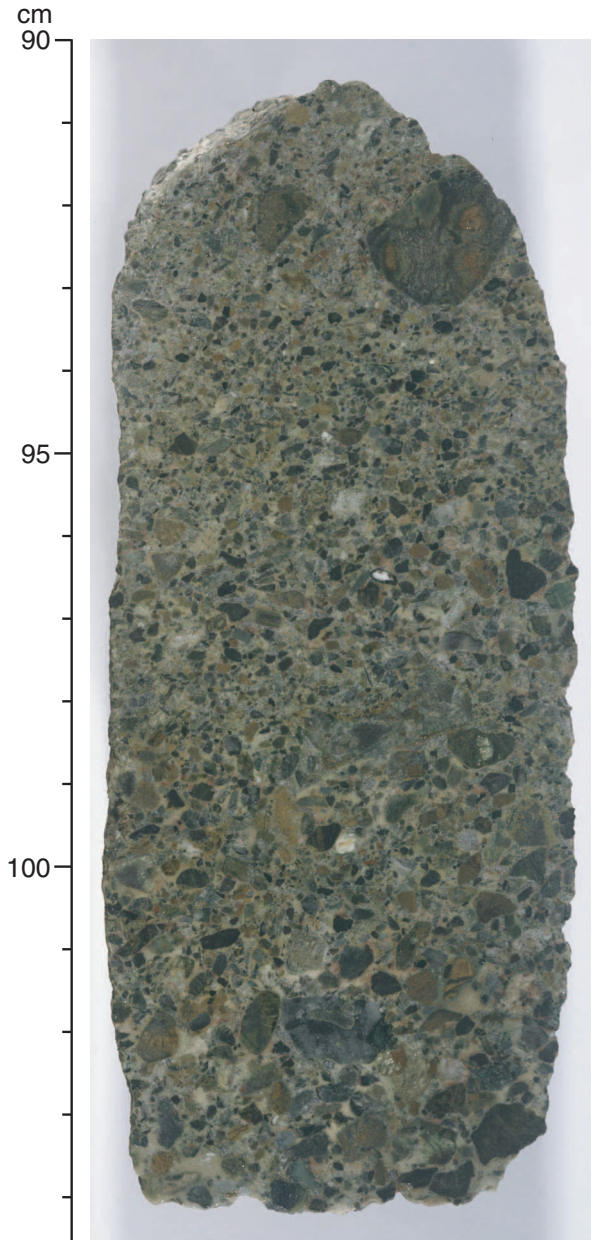

Figure F9. Hyaloclastite cut by an inferred neptunian fissure (white; lower left side) (interval 210-1277A-1W-1, 29–61 cm). The fissure is filled with polymict clastic sediments (57–59 cm) with a sparry calcite cement (white).

Figure F10. Well-laminated and graded sandstone cut by calcite-filled fractures (interval 210-1277A-5R-2, 32–43 cm). This sandstone is composed of subrounded, well-sorted serpentinite and gabbro grains.

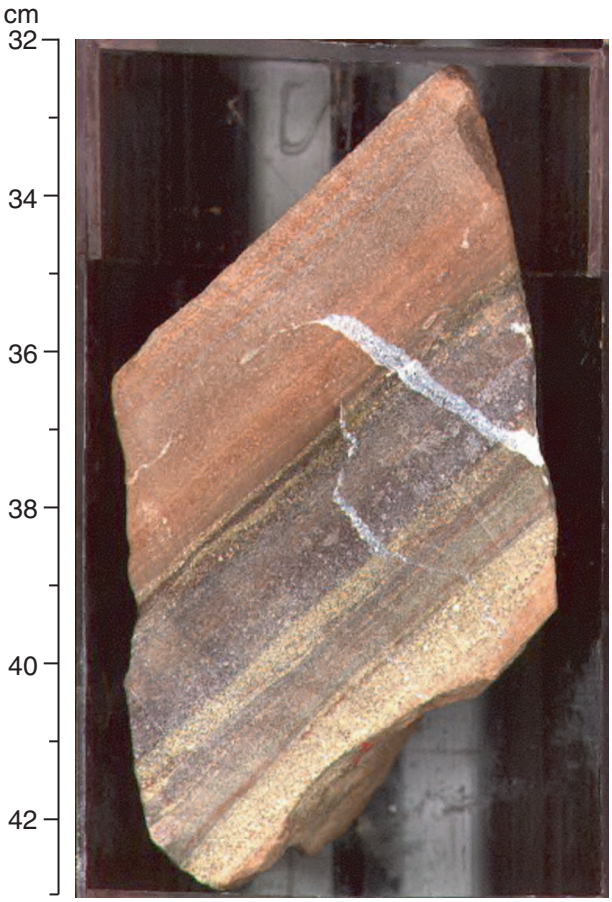

Figure F11. Foliated serpentinized peridotite (dark) cut by a network of anastomosing paler greenish veins consisting of calcite and talc (interval 210-1277A-7R-2, 111–124 cm).

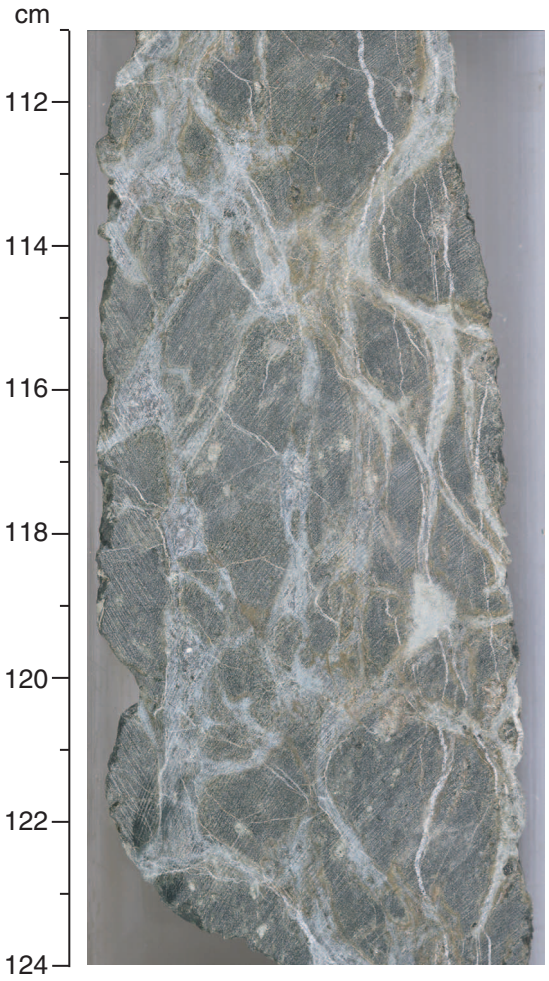

Figure F12. Foliated serpentinized peridotite (interval 210-1277A-9R-4, 26–46 cm). The foliation is defined by elongate aggregates of recrystallized pyroxene, which together with pyroxene porphyroblasts define an early high-temperature mylonite fabric. The subvertical orientation of this foliation and the postkinematic serpentinization suggest that the fabric is unlikely to be related to the final exhumation of the mantle rocks to the seafloor. The vertical hairline cracks are filled with calcite and resulted from later deformation at or near the seafloor.

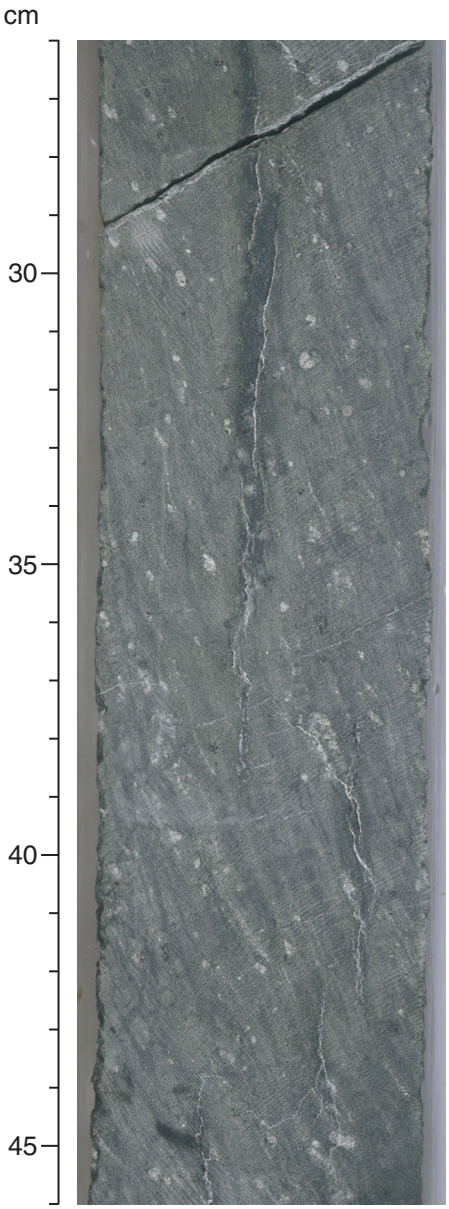

Figure F13. Serpentinized peridotite preserving a high-temperature foliation cut by several generations of calcite veins (interval 210-1277A-9R-3, 1–30 cm).

Figure F14. Serpentinized peridotite cut by plagioclase-bearing magmatic veins (top and lower left) (interval 210-1277A-9R-1, 1–19 cm). Sparry calcite veins appear at the contacts between the magmatic intrusive rocks and the serpentinites.

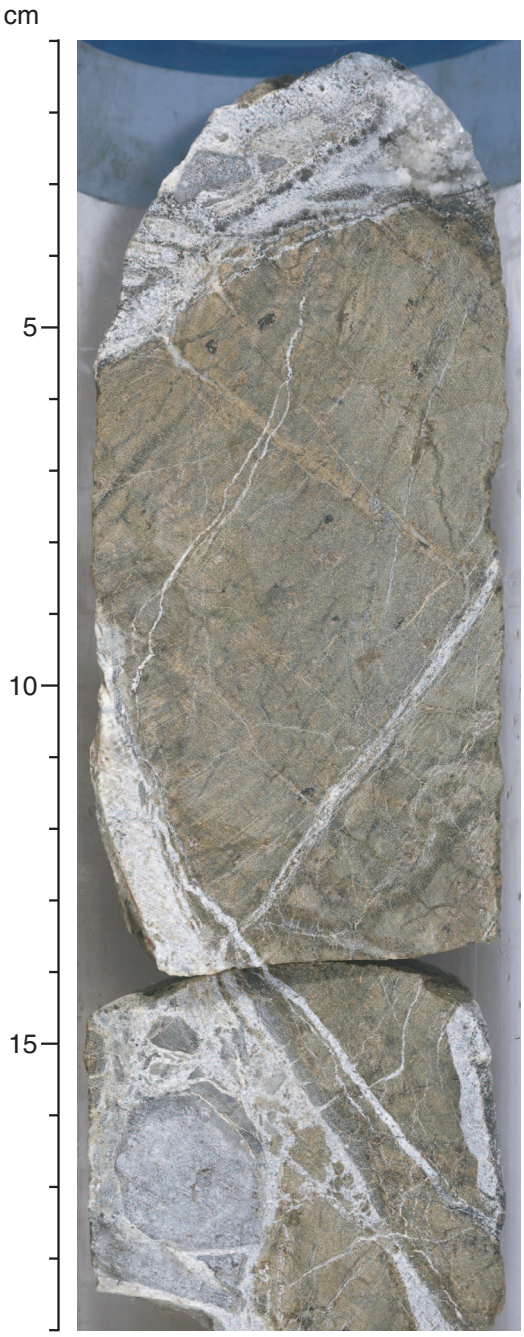

Figure F15. Plots of magnetic susceptibility measured with the point-susceptibility meter (archive multisensor track) and remanent magnetization intensity and inclination before and after 20-mT AF demagnetization for cores in Hole 1277A. NRM = natural remanent magnetization.

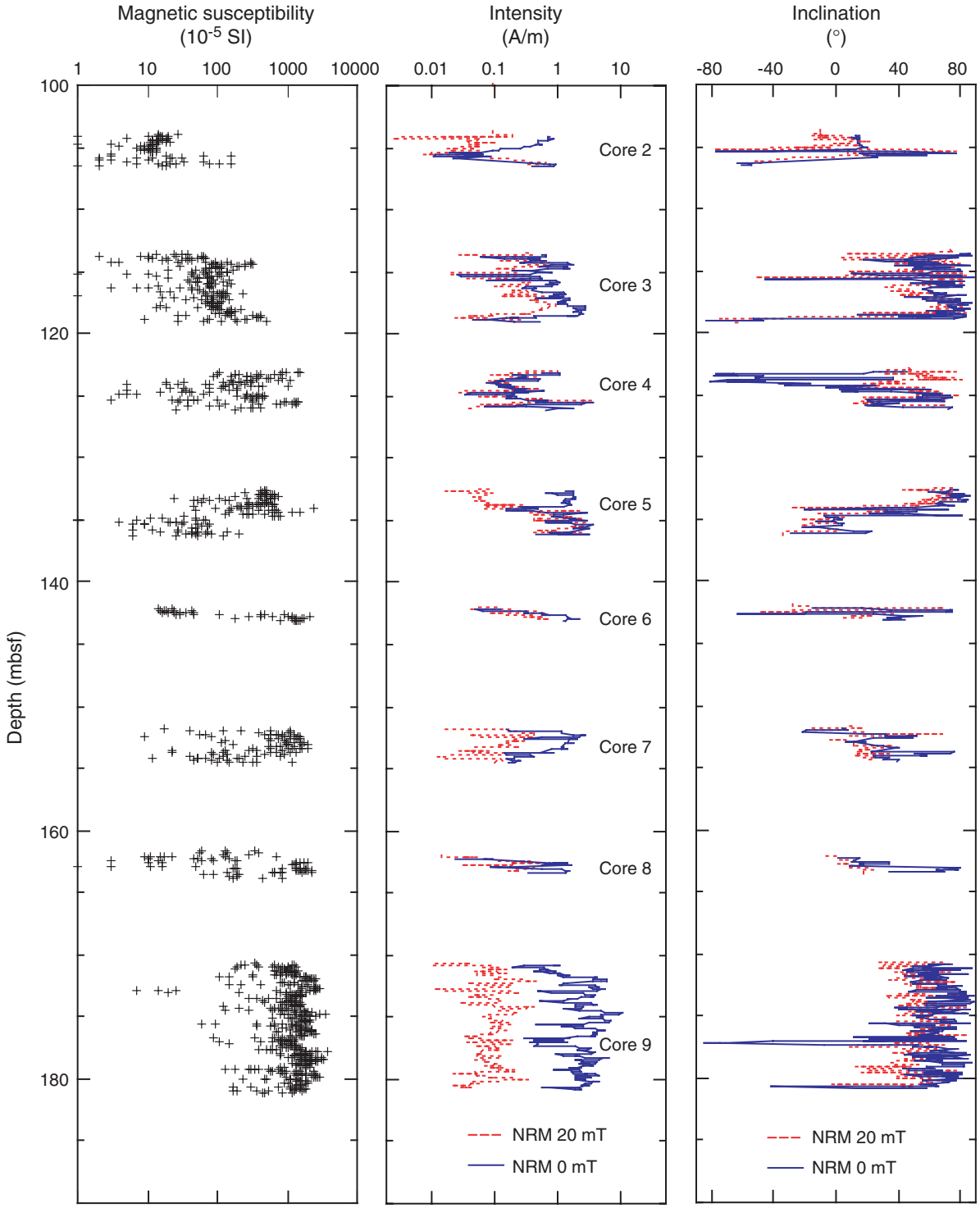

Figure F16. Examples of Zijderveld diagrams for cores recovered from Hole 1277A showing the removal of a normal component of remagnetization and the isolation of a more stable component that is decaying toward the origin (Zijderveld, 1967). Open and solid squares represent vector endpoints projected onto the vertical and horizontal planes, respectively. NRM = natural remanent magnetization.

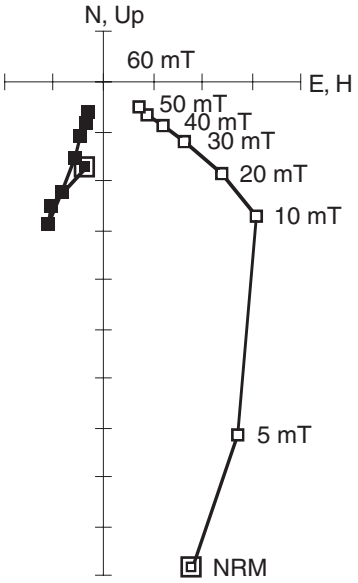

Sample 210-1277A-1W-2, 100 cm
Mafic breccia

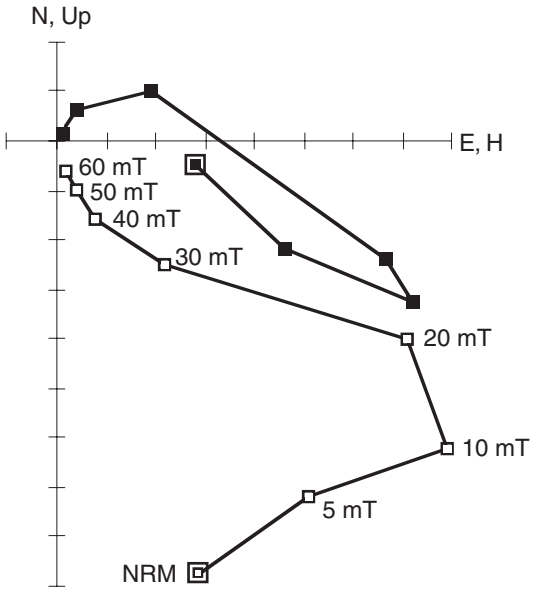

Sample 210-1277A-5R-2, 24 cm
Gabbro

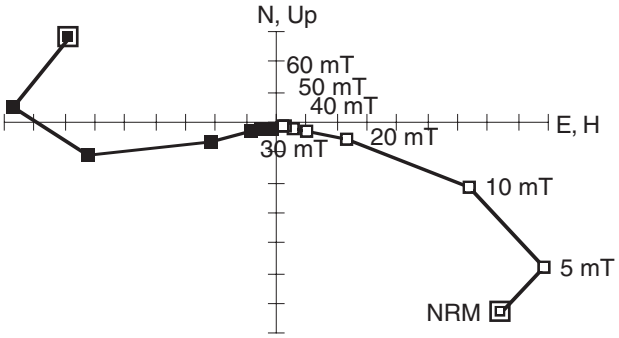

Sample 210-1277A-7R-1, 82 cm
Vesicular basalt

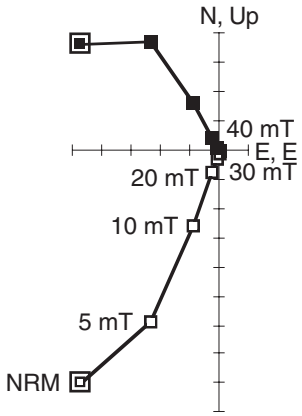

Sample 210-1277A-9R-3, 78 cm
Serpentinized peridotite

Figure F17. Bulk density, grain density, and porosity from MAD measurements. Core recovery is shown at left.

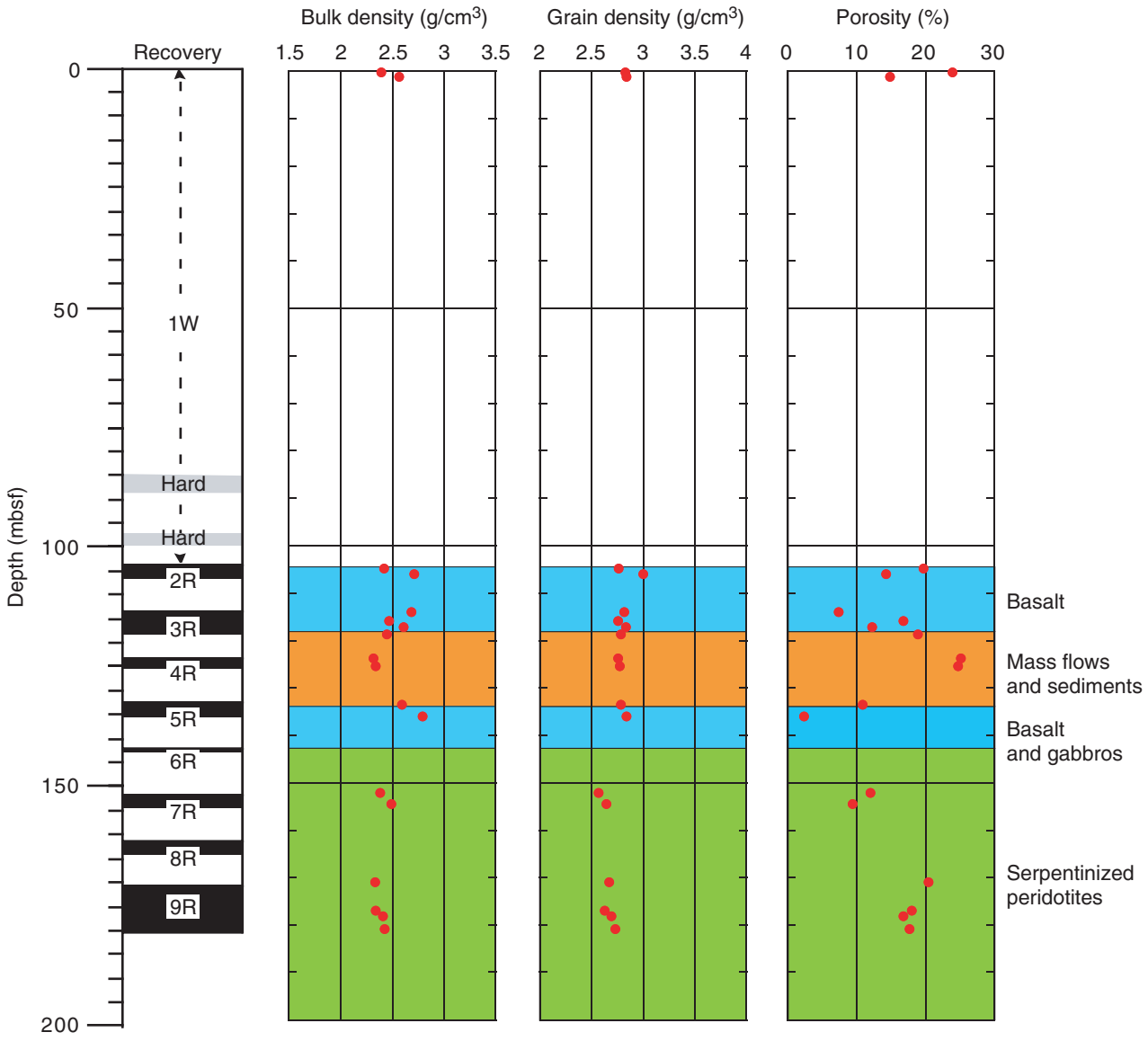

Figure F18. *P*-wave velocity (x-, y-, and z-directions), measured using the PWS3 contact probe system. Core recovery is shown at left.

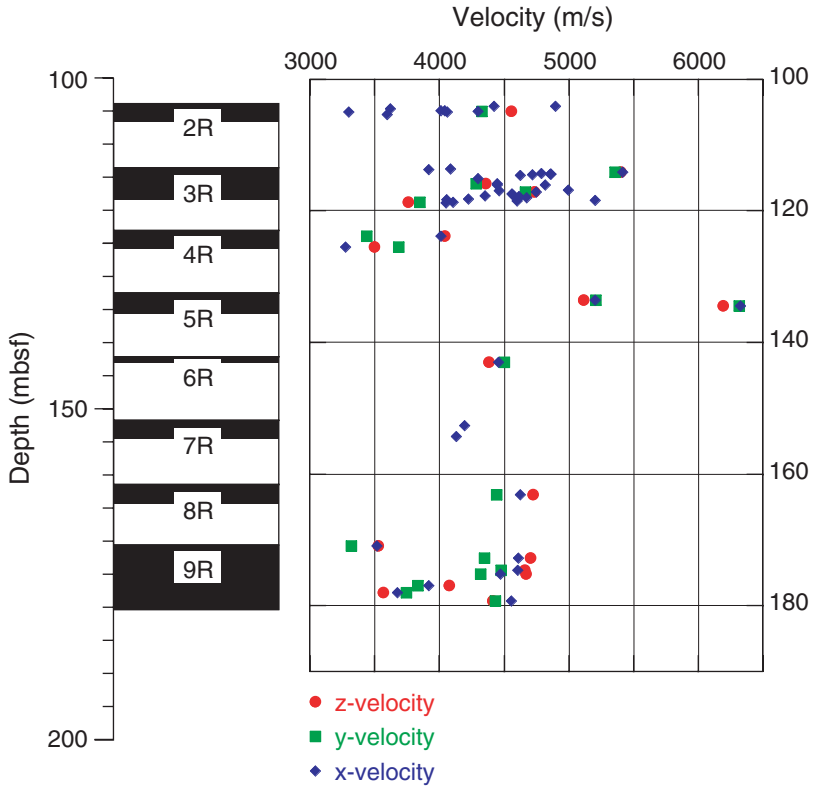

Figure F19. Thermal conductivity vs. depth. Core recovery is shown at left.

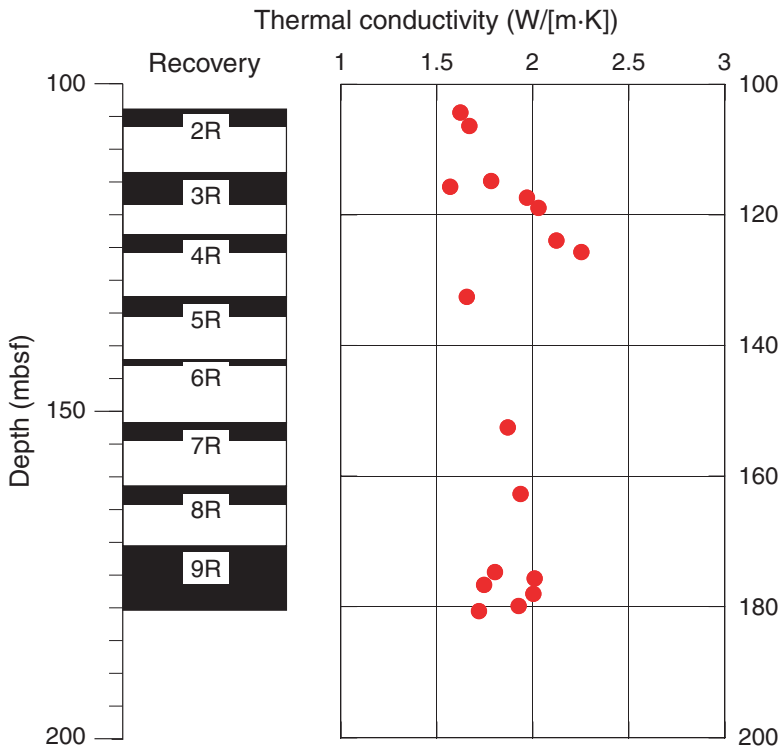

Figure F20. Time-migrated seismic reflection sections showing Study of Continental Rifting and Extension on the Eastern Canadian Shelf (SCREECH) lines 2MCS and 206 where they cross at Site 1277. Positive reflection amplitudes are red to yellow, and negative amplitudes are gray to black. The black line approximates the depth of basement penetration. For line locations, see Figure F6, p. 46, in the "Leg 210 Summary" chapter. CMP = common midpoint.

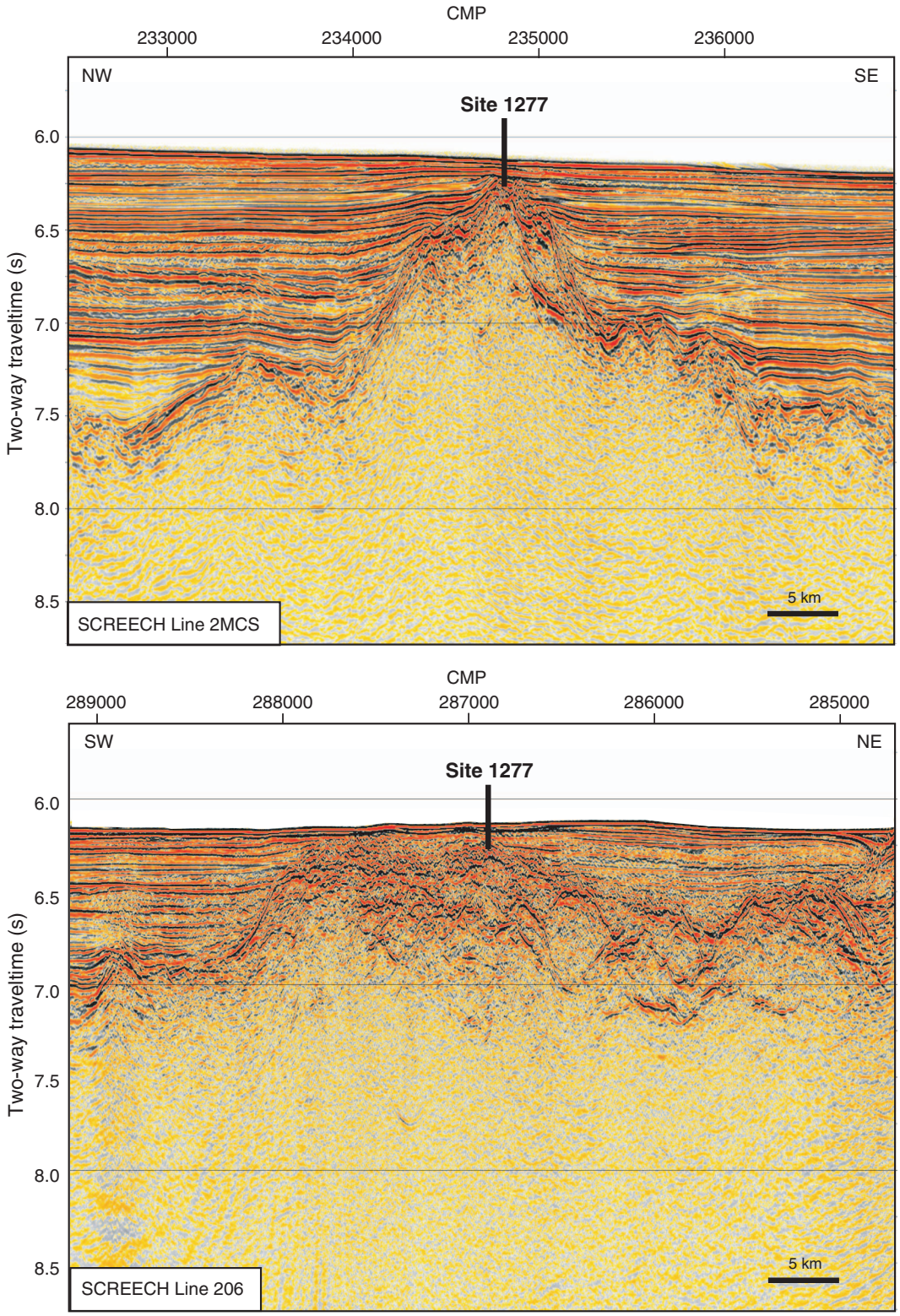

Figure F21. Close-up of time-migrated seismic reflection section of Study of Continental Rifting and Extension on the Eastern Canadian Shelf (SCREECH) line 2MCS at Site 1277. Positive reflection amplitudes are red to yellow, and negative amplitudes are gray to black. The black line approximates the depth of basement penetration. Note the irregularly "layered" character of the uppermost basement. CMP = common midpoint.

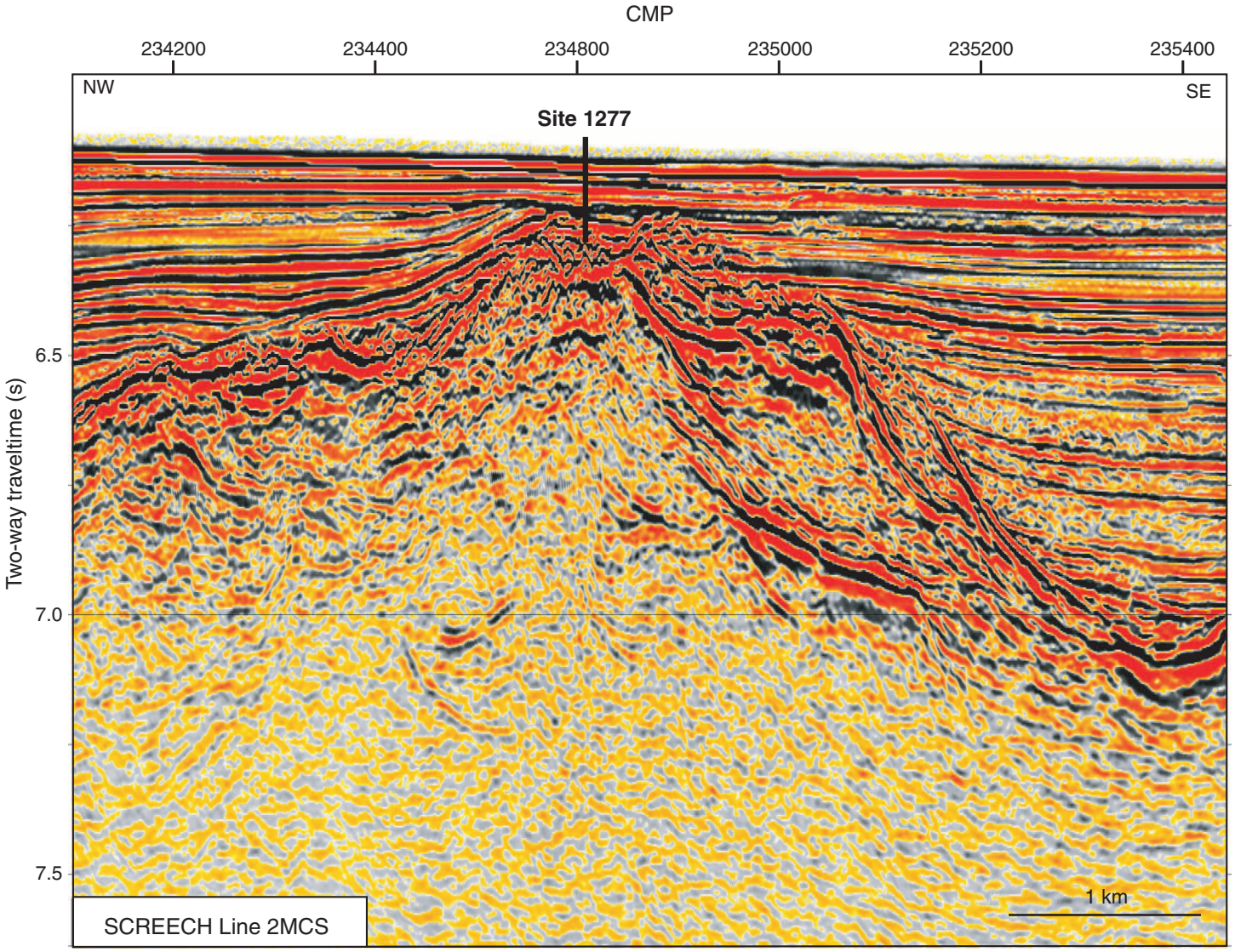

Table T1. Site 1277 coring summary.

Hole 1277A
Latitude: 45°11.8002′N
Longitude: 44°22.5999′E
Time on site: 55 hr (1800 hr, 2 Sep–0100 hr, 5 Sep 2003)
Seafloor (drill pipe measurement from rig floor, mbrf): 4639.4
Distance between rig floor and sea level (m): 11.2
Water depth (drill pipe measurement from sea level, m): 4628.2
Total depth (drill pipe measurement from rig floor, mbrf): 4819.7
Total penetration (m): 180.3
Total length of cored section (m): 76.4 (103.9–180.3 mbsf)
Total core recovered (m): 29.24 (not including 2.29 m from wash Core 210-1277A-1W)
Core recovery (%): 38
Total number of cores: 8
Total number of drilled intervals: 1 (0–103.9 mbsf)
Total length of drilled interval without coring (m): 103.9

Core	Date (Sep 2003)	Local time (hr)	Depth (mbsf) Top	Depth (mbsf) Bottom	Length (m) Cored	Length (m) Recovered	Recovered (%)	Comment
210-1277A-								
1W	3	1050	*****Drilled without coring from 0 to 103.9 mbsf*****					2.29 m recovered in wash core
2R	3	1315	103.9	113.6	9.7	2.43	25	
3R	3	1640	113.6	123.0	9.4	4.65	49	
4R	3	2000	123.0	132.6	9.6	2.83	29	
5R	3	2300	132.6	142.1	9.5	3.02	31	
6R	4	120	142.1	151.8	9.7	0.90	9	
7R	4	425	151.8	161.5	9.7	2.60	26	
8R	4	810	161.5	170.7	9.2	2.66	28	
9R	4	1215	170.7	180.3	9.6	10.15	105	Last core of Leg 210 and ODP
				Total:	76.4	29.24	38	

Table T2. Remanent magnetization intensity and inclination, Hole 1277A.

Leg	Hole	Core	Section	Top (cm)	Depth (mbsf)	Inc (°)	NRM_Int (A/m)
210	1277	1	1	12	0.12*	8.93	0.74
210	1277	1	1	14	0.14*	6.11	0.977
210	1277	1	1	16	0.16*	3.35	0.942
210	1277	1	1	18	0.18*	0.85	0.661
210	1277	1	1	20	0.2*	–1.78	0.357
210	1277	1	1	22	0.22*	–1.76	0.252
210	1277	1	1	24	0.24*	6.4	0.349
210	1277	1	1	26	0.26*	16.4	0.564
210	1277	1	1	28	0.28*	17.7	1.26
210	1277	1	1	30	0.3*	18.67	2.37
210	1277	1	1	32	0.32*	21.93	3.27
210	1277	1	1	34	0.34*	28.44	3.41
210	1277	1	1	36	0.36*	38.92	2.67
210	1277	1	1	38	0.38*	51.31	1.67
210	1277	1	1	40	0.4*	53.94	1.01
210	1277	1	1	42	0.42*	48.28	0.623
210	1277	1	1	44	0.44*	49.89	0.417
210	1277	1	1	46	0.46*	43.11	0.466
210	1277	1	1	48	0.48*	50.5	0.526
210	1277	1	1	50	0.5*	69.29	0.497
210	1277	1	1	52	0.52*	61.2	0.451
210	1277	1	1	54	0.54*	31.84	0.457
210	1277	1	1	56	0.56*	12.36	0.441
210	1277	1	1	58	0.58*	–3.94	0.436
210	1277	1	1	60	0.6*	–20.44	0.445
210	1277	1	1	70	0.7*	14.66	1.52
210	1277	1	1	72	0.72*	23.36	2
210	1277	1	1	74	0.74*	29.52	2.43
210	1277	1	1	76	0.76*	36.32	2.73
210	1277	1	1	78	0.78*	45.35	2.8
210	1277	1	1	80	0.8*	52.78	2.69
210	1277	1	1	82	0.82*	57.3	2.58
210	1277	1	1	84	0.84*	60.27	2.64
210	1277	1	1	86	0.86*	60.18	2.95
210	1277	1	1	88	0.88*	62.08	3.33
210	1277	1	1	90	0.9*	65.48	3.69
210	1277	1	1	92	0.92*	68.41	4.02
210	1277	1	1	94	0.94*	71.72	4.16
210	1277	1	1	96	0.96*	75.28	4.17
210	1277	1	1	98	0.98*	76.82	3.88
210	1277	1	1	100	1*	68.61	3.43
210	1277	1	1	102	1.02*	57.11	2.97
210	1277	1	1	104	1.04*	53.06	2.32
210	1277	1	1	106	1.06*	65.79	1.45
210	1277	1	1	108	1.08*	66.27	1.35
210	1277	1	1	110	1.1*	42.36	2.39
210	1277	1	1	112	1.12*	37.01	3.5
210	1277	1	1	114	1.14*	38.47	4.25
210	1277	1	1	116	1.16*	47.11	4.25
210	1277	1	1	118	1.18*	63.09	3.53
210	1277	1	1	120	1.2*	81.88	2.58
210	1277	1	1	122	1.22*	80.6	1.92
210	1277	1	1	124	1.24*	78.98	1.4
210	1277	1	1	126	1.26*	46.64	1.84
210	1277	1	1	128	1.28*	38.96	2.74
210	1277	1	1	130	1.3*	44.26	3.12
210	1277	1	2	6	1.42*	62.76	2.09
210	1277	1	2	8	1.44*	63.93	2.36
210	1277	1	2	10	1.46*	64.6	2.58
210	1277	1	2	12	1.48*	66.64	2.89
210	1277	1	2	14	1.5*	70.89	3.2
210	1277	1	2	16	1.52*	76.66	3.36
210	1277	1	2	18	1.54*	80.75	3.36

Notes: NRM_Int = remanent magnetization intensity, Inc = inclination. * = distance from the core top in meters; taken from a wash core. Only a portion of this table appears here. The complete table is available in **ASCII**.

Table T3. Magnetic susceptibility measured with the point-susceptibility meter (AMST), Hole 1277A.

Leg	Site	Hole	Core	Type	Section	Top (cm)	Depth (mbsf)	Magnetic Susceptibility (10^{-5} SI)
210	1277	A	1	W	1	6	0.06*	19
210	1277	A	1	W	1	12	0.12*	260
210	1277	A	1	W	1	14	0.14*	460
210	1277	A	1	W	1	16	0.16*	404
210	1277	A	1	W	1	22	0.22*	60
210	1277	A	1	W	1	24	0.24*	216
210	1277	A	1	W	1	26	0.26*	327
210	1277	A	1	W	1	32	0.32*	254
210	1277	A	1	W	1	34	0.34*	348
210	1277	A	1	W	1	36	0.36*	228
210	1277	A	1	W	1	38	0.38*	199
210	1277	A	1	W	1	40	0.4*	21
210	1277	A	1	W	1	42	0.42*	139
210	1277	A	1	W	1	44	0.44*	275
210	1277	A	1	W	1	46	0.46*	137
210	1277	A	1	W	1	48	0.48*	176
210	1277	A	1	W	1	50	0.5*	149
210	1277	A	1	W	1	52	0.52*	162
210	1277	A	1	W	1	54	0.54*	171
210	1277	A	1	W	1	56	0.56*	206
210	1277	A	1	W	1	58	0.58*	72
210	1277	A	1	W	1	60	0.6*	35
210	1277	A	1	W	1	64	0.64*	84
210	1277	A	1	W	1	68	0.68*	528
210	1277	A	1	W	1	70	0.7*	557
210	1277	A	1	W	1	72	0.72*	503
210	1277	A	1	W	1	74	0.74*	452
210	1277	A	1	W	1	76	0.76*	422
210	1277	A	1	W	1	78	0.78*	413
210	1277	A	1	W	1	80	0.8*	416
210	1277	A	1	W	1	82	0.82*	404
210	1277	A	1	W	1	84	0.84*	472
210	1277	A	1	W	1	90	0.9*	544
210	1277	A	1	W	1	92	0.92*	553
210	1277	A	1	W	1	94	0.94*	543
210	1277	A	1	W	1	96	0.96*	533
210	1277	A	1	W	1	98	0.98*	527
210	1277	A	1	W	1	100	1*	519
210	1277	A	1	W	1	102	1.02*	402
210	1277	A	1	W	1	104	1.04*	320
210	1277	A	1	W	1	108	1.08*	256
210	1277	A	1	W	1	110	1.1*	410
210	1277	A	1	W	1	112	1.12*	354
210	1277	A	1	W	1	114	1.14*	425
210	1277	A	1	W	1	116	1.16*	442
210	1277	A	1	W	1	118	1.18*	361
210	1277	A	1	W	1	122	1.22*	217
210	1277	A	1	W	1	124	1.24*	186
210	1277	A	1	W	1	126	1.26*	293
210	1277	A	1	W	1	128	1.28*	521
210	1277	A	1	W	1	130	1.3*	536
210	1277	A	1	W	2	4	1.4*	497
210	1277	A	1	W	2	6	1.42*	512
210	1277	A	1	W	2	8	1.44*	496
210	1277	A	1	W	2	10	1.46*	547
210	1277	A	1	W	2	12	1.48*	497
210	1277	A	1	W	2	14	1.5*	398
210	1277	A	1	W	2	16	1.52*	544
210	1277	A	1	W	2	18	1.54*	525
210	1277	A	1	W	2	20	1.56*	539
210	1277	A	1	W	2	22	1.58*	552
210	1277	A	1	W	2	24	1.6*	565
210	1277	A	1	W	2	26	1.62*	538

Notes: AMST = archive multisensor track. W= wash core, R = rotary core barrel. * = distance from the core top in meters. Only a portion of this table appears here. The complete table is available in **ASCII**.

Table T4. Remanent magnetization intensity, magnetic susceptibility, MDFs, and *Q*, Hole 1277A.

Leg	Site	Hole	Core	Type	Section	Top (cm)	Depth (mbsf)	Magnetic susceptibility (10^{-5} SI)	NRM_Int (A/m)	MDF (mT)	*Q*
210	1277	A	1	W	1	108	1.08	256	1.35	8	13.32
210	1277	A	1	W	2	24	1.6	565	3.62	5	16.18
210	1277	A	1	W	2	100	2.36	347	0.428	7.5	3.12
210	1277	A	2	R	1	28	104.18	20	0.691	15	87.27
210	1277	A	2	R	1	114	105.04	10	0.215	15	54.31
210	1277	A	5	R	2	8	134.11	2346	0.156	28	0.17
210	1277	A	5	R	2	12	134.15	644	0.155	20	0.61
210	1277	A	5	R	2	24	134.27	689	0.238	28.5	0.87
210	1277	A	5	R	2	26	134.29	379	0.374	28	2.49
210	1277	A	5	R	2	30	134.33	761	0.698	25	2.32
210	1277	A	5	R	2	66	134.69	598	1.07	22	4.52
210	1277	A	7	R	1	56	152.36	475	2.25	12	11.96
210	1277	A	7	R	1	64	152.44	1490	1.33	10	2.25
210	1277	A	7	R	1	82	152.62	548	1.23	14	5.67
210	1277	A	7	R	1	110	152.9	1539	1.34	10	2.20
210	1277	A	7	R	2	46	153.69	1379	0.855	7	1.57
210	1277	A	7	R	2	58	153.81	87	0.152	15	4.41
210	1277	A	7	R	2	74	153.97	247	0.41	19	4.19
210	1277	A	7	R	2	90	154.13	187	0.208	6	2.81
210	1277	A	7	R	2	118	154.41	139	0.232	25	4.22
210	1277	A	8	R	1	78	162.28	52	0.089	21	4.32
210	1277	A	8	R	1	112	162.62	2016	1.39	15	1.74
210	1277	A	8	R	1	124	162.74	1205	1.56	19.5	3.27
210	1277	A	8	R	1	142	162.92	48	0.023	49	1.21
210	1277	A	8	R	2	24	163.19	1962	1.49	8	1.92
210	1277	A	8	R	2	42	163.37	851	0.832	12	2.47
210	1277	A	8	R	2	46	163.41	666	0.513	20	1.95
210	1277	A	8	R	2	48	163.43	612	0.349	20	1.44
210	1277	A	9	R	3	30	173.97	1575	4.03	4	6.46
210	1277	A	9	R	3	64	174.31	749	1.55	7	5.23
210	1277	A	9	R	3	70	174.37	636	1.21	12	4.81
210	1277	A	9	R	3	76	174.43	605	2.88	9.8	12.02
210	1277	A	9	R	3	120	174.87	2618	4.69	5	4.52
210	1277	A	9	R	4	18	175.19	1617	5.42	4.5	8.47
210	1277	A	9	R	4	50	175.51	1140	2.54	9.7	5.63
210	1277	A	9	R	4	62	175.63	660	1.9	9.8	7.27
210	1277	A	9	R	4	120	176.21	1354	3.65	7	6.81
210	1277	A	9	R	5	58	177	1232	1.4	9.8	2.87
210	1277	A	9	R	5	66	177.08	952	0.436	10	1.16
210	1277	A	9	R	5	86	177.28	1305	0.505	16	0.98
210	1277	A	9	R	5	92	177.34	1266	1.21	7.5	2.41
210	1277	A	9	R	6	10	177.82	2661	3.19	4	3.03
210	1277	A	9	R	6	44	178.16	1543	1.93	5	3.16
210	1277	A	9	R	6	124	178.96	1811	2.96	5	4.13
210	1277	A	9	R	7	8	179.16	732	1.61	6.8	5.56
210	1277	A	9	R	7	38	179.46	571	1.63	4.9	7.21
210	1277	A	9	R	7	66	179.74	1343	2.04	4.7	3.84
210	1277	A	9	R	7	88	179.96	1471	2.7	5	4.64
210	1277	A	9	R	7	122	180.3	1933	3.02	4.6	3.95
210	1277	A	9	R	8	14	180.51	1410	2.92	5	5.23
210	1277	A	9	R	8	24	180.61	1301	1.49	5	2.89
210	1277	A	9	R	8	40	180.77	1345	1.88	3.5	3.53

Notes: NRM_Int = remanent magnetization intensity, MDF = median destructive field, *Q* = Königsberger ratio. W = wash core, R = rotary core barrel.